R. & M. No. 2846
(14,509)
A.R.C. Technical Report

MINISTRY OF SUPPLY

AERONAUTICAL RESEARCH COUNCIL
REPORTS AND MEMORANDA

Alternating Pressures and Blade Stresses in an Axial-Flow Compressor

By

J. R. FORSHAW, M.Eng.,
H. TAYLOR, B.Sc.,
and
R. CHAPLIN, B.Sc.

LONDON: HER MAJESTY'S STATIONERY OFFICE
1956
EIGHT SHILLINGS NET

Alternating Pressures and Blade Stresses in an Axial-Flow Compressor

By

J. R. FORSHAW, M.Eng.,
H. TAYLOR, B.Sc.,
and
R. CHAPLIN, B.Sc.

COMMUNICATED BY THE PRINCIPAL DIRECTOR OF SCIENTIFIC RESEARCH (AIR), MINISTRY OF SUPPLY

Reports and Memoranda No. 2846*

June, 1951

Summary.—The majority of blade failures in axial-flow compressors have occurred in the rotor blades of the lower pressure stages. These have been caused mainly by fatigue in the fundamental flexural mode of vibration in the presence of the steady centrifugal and gas bending stresses.

An investigation has been made into the origin of the forces exciting vibration in an axial-flow compressor, and their magnitude relative to the calculated gas bending loads. The blade stresses resulting from these forces were measured, and a value obtained for the energy input to a blade when vibrating in the predominant modes under running conditions.

The experimental data were obtained from pressure elements and strain-gauges fitted to the inlet guide vanes and first four stator-blade rows of an early compressor.

The oscillating pressure reached peak values when the forcing frequencies in a stage coincided with the blade natural frequencies of that stage or of adjacent stages, and was predominant for modes approximating to the fundamental flexural mode of vibration. This indicated that vibrations of any one stage 'modulated' the stream, the pressure waves extending upstream and downstream.

The magnitude of the alternating pressure was 40 per cent and 5 per cent of the stage pressure rise at 4,000 and 8,000 r.p.m. respectively. The ratio of the major harmonic components of the alternating stress to the calculated gas bending stress was 2:1·3 : 0·6 at rotor speeds of 4,000, 6,000 and 8,000 r.p.m.

Values of input energy and kinetic energy obtained for resonances approximating to the fundamental flexural mode showed that the damping present in a stator blade was high. Contributing factors to this high damping were the light root platform and loose fit of some blades.

The prominence of blade vibration resulting from modulation of the air stream by the vibration of blades in adjacent stages is attributed to the high damping present.

1. *Introduction.*—Blade failures in axial-flow compressors have occurred mainly in the rotor blades of the lower pressure stages. Stresses resulting from vibration of the blades in their fundamental flexural mode superimposed upon the centrifugal and gas bending stresses have been the major cause of failure.

* N.G.T.E. Report R.92, received 28th December, 1951.

An early design of axial-flow compressor was employed for the investigation having design performance:

Mass flow	50 lb/sec	
Compression ratio	5:1	
Design speed	8,000 r.p.m.	
Number of stages	14	
Number of inlet spiders	11	
Number of stator blades	38	For each of first five stages
Number of rotor blades	36	
Blade material	RR 56	

Capacitance-type pressure elements were fitted to an inlet guide vane and one of each of the first four stator rows together with wire-resistance strain-gauges, to study the exciting forces and resulting blade loads.

The compressor was run as a component of a jet propulsion unit with atmospheric inlet, the pressure bearing a definite relation to speed.

Information required for calculations on the flow through the compressor was obtained from the design data and published cascade results.

The results of the investigation have been presented in a manner suitable for general application.

2. *Description of Measuring Elements and Recording Equipment.*—2.1. *Design of Pressure-Measuring Element.*—The pressure-measuring element was of the capacitance type and an early design is shown in Fig. 1. A hole was drilled through the aerofoil section of the compressor blade and a steel outer case was peened in position in the Duralumin blade. A steel disc was assembled in the outer case and insulated from it with Bakelised fabric, to form one plate of a condenser. The earthy plate was formed by the diaphragm 0·5-in. diam. and 0·003-in. thick which was spot-welded to the steel outer case. The 0·002-in. gap between the two plates of the condenser contained a 0·001-in. thick sheet of mica, leaving an air gap of 0·001 in. on assembly, to permit diaphragm movement. A P.V.C. insulated wire was soldered to the insulated plate and passed through a $\frac{1}{16}$-in. diam. hole drilled the length of the blade. The contour of the lower pressure face of the blade was retained by filling with a Bakelite cement.

Leakage between the spot-welding of the diaphragm and outer case affected the response of the element to alternating pressures at low frequencies. In the second design, shown in Fig. 2, the pressure element was made as a sealed cylindrical capsule 0·5-in. diam., 0·040-in. thick. The same diaphragm and plate spacing was used as in the first design but the diaphragm was soldered to the outer case. A flat-bottomed hole was drilled in the concave face of the blade to take the capsule which was retained in position by Bakelite cement. The diaphragm was approximately flush with the surface. The lead-out wire was again passed through a hole drilled the length of the blade and a satisfactory calibration obtained.

2.2. *Calibration of Pressure-Measuring Element.*—A typical static-pressure calibration of an element is given in Fig. 3. To obtain a dynamic-pressure calibration the output of the element mounted in a blade was determined by using a loudspeaker as the source of oscillating pressure waves, and comparing the element output with that of a standard microphone. The calibration curve for the pressure element in the first-stage stator blade is given in Fig. 4. All readings were corrected on this basis up to a frequency of 14,500 c.p.s. above which the dynamic response was assumed to be identical with the static value.

2.3. *Installation of Pressure Elements and Strain-Gauges in the Compressor.*—A pressure element was fitted in one stator blade of each of the first four stages and in an inlet guide vane at 0·85 length of the blade. This position was selected on mechanical considerations and was also convenient in relation to the pressure distribution around the aerofoil section. The lead-out wire passed through the root platform, the filling slot in the compressor outer casing being milled locally to pass the wire to a hole in the outer casing which had been drilled in a suitable position.

Wire-resistance strain-gauges of 50 ohms resistance consisting of a fine wire grid 8 mm long and 1·5 mm wide were cemented at two positions to the convex face of other blades in the same rows. These were located at 0·85 length of the blade and 0·375 in. from the root platform respectively.

Thermocouples and static-pressure points were placed in other blades in the same rows at 0·85 of the length of the blades.

Some of the strain elements in position on the compressor are shown in Fig. 5.

2.4. *Installation of Engine and Electronic Equipment.*— The engine was installed in the test cell on the usual suspension as shown in the two views of Fig. 6. The lead-out wires from the capacitance-type pressure elements are shown passing to their adjacent oscillators ; leads from the wire-resistance strain-gauges and oscillators can be seen passing to the control room.

The pressure channels employed a frequency modulation system of capacitance measurement and could interpret alternating or steady pressure quantities ; the strain-gauge channels measured alternating strain only.

Fig. 7 shows the electronic equipment in position in the control room. The frequency modulated circuits for the condenser elements are lettered A, strain-gauge amplifier B, d.c. amplifier C and recording cameras D, E, F and G.

2.5. *Recording Cameras.*—Signals from the various elements, and in particular the pressure elements, contained harmonic component frequencies ranging from low audio frequencies up to 30,000 c.p.s. in some instances. Throughout the experiments each signal was recorded in four cameras namely:

D	35-mm moving-film camera	50 in./sec
E	35-mm mechanically reloading drum camera	400 in./sec
F	70-mm drum camera	600 in./sec
G	70-mm single-stroke camera	2,500 in./sec.

Particular harmonic components were resolved from the camera record with the most convenient film speed, and a typical signal recorded by the four cameras is shown in Fig. 8.

3. *Description of Experiments.*—It was necessary to run the engine for some time to develop the technique for the experiment and one delay was caused by a mechanical failure. Some of the elements became unserviceable before a complete set of readings could be taken. Analysis has been concentrated on the readings from the first-stage pressure element and of the strain readings from the first and fourth-stage stator blades. Readings were taken over a speed range of 3,500 r.p.m. to 8,000 r.p.m. in steps of 500 r.p.m. The temperature rise in the later stages caused distortion of the Bakelised fabric insulating material in the pressure element with subsequent electrical breakdown. This effect could have been eliminated by the use of an insulator with improved properties at these temperatures.

4. *Discussion of Results.*—4.1. *Harmonic Analysis of Records.*—During one of the early runs an analysis was made of the signal from the first-stage pressure element using the General Radio Sound Analyser type 760A (Fig. 9). Visual analysis of the records gave a more comprehensive analysis, however, and this method was used throughout the investigation.

Analyses of the predominant harmonic components of the signals from the pressure elements and wire-resistance strain-gauges are given in the following figures:

Fig. 10. Predominant harmonic components of oscillating pressure at 0·85 length of 1st stage stator blade.

Fig. 11. Predominant harmonic components of stress at root of 1st stage stator blade.

Fig. 12. Predominant harmonic components of stress at 0·85 length of 1st stage stator blade.

Fig. 13. Predominant harmonic components of stress at root of 4th stage stator blade.

Fig. 14. Predominant harmonic components of stress at 0·85 length of 4th stage stator blade.

Analysis of the oscillating pressures and strains showed that the exciting orders could be grouped in the following manner:

Source of excitation	Alternating pressure 1st stage	Alternating Strain			
		1st stage		4th stage	
		Root	Tip	Root	Tip
1. Non-uniform entry	1, 2, 4, 5, 6, 7, 8, 18	3, 4, 5, 6, 7, 8	1, 2, 6	6, 7, 8, 9, 10	1, 2, 4, 7, 8, 9
2. Intake spider	33, 44, 77, 88	22	22	11	11, 44
3. Rotor blades passing stator blades	36, 72, 108, 144, 180, 216, 252	36, 72	36, 72	36, 72	36, 72

A particular wake or disturbance will reduce in intensity as it passes downstream.

Due to the geometry of the compressor some orders will be in phase when summated around the circumference as shown in Ref. 4 and Appendix I. If n is the number of blades in a row and m any integer, an axial effect, *i.e.*, a stationary wave in the compressor annulus will result from the addition of orders $m \times n$.

The resultant in an axial direction for Groups 1 and 2 when summated will be zero, and initial impulses of these orders will not be sustained. Additional excitation may be set up through the compressor, however, due to a lack of symmetry, or through disturbances in the flow.

The orders listed in Group 3 are those resulting from rotor blades passing stator blades which are in phase when summated. Orders in this category which should in theory summate to zero or produce forward or reverse couples were not detected.

The higher orders predominated at the lower compressor speeds and airflows, indicating irregular airflows for those conditions.

4.2. *Discussion of Results.*—Analyses of the strain and pressure readings indicated that the blade was more responsive to the lower frequency excitation. The differing response of root and tip sections to a particular frequency or mode is clearly shown by a comparison of Figs. 11 and 12, and Figs. 13 and 14.

Blade natural mode frequencies were determined in the laboratory for the inlet guide vane and first four compressor stages and are given in Table 1.

Analyses of the pressure and strain readings were of the same form and could have resulted from seismic response of the pressure element. Further examination showed however that the shape of the curves for a particular order was different and that pressure peaks occurred at frequencies other than the natural frequencies of the particular blade.

There are a number of instances where a blade had peak stresses forced by two different orders at the same compressor speed each exciting a mode which was mainly fundamental flexure.

5th and 6th orders 1st stage root strains at 5,010 r.p.m.
gives frequencies 417 and 510 c.p.s.

5th and 7th orders 1st stage root strains at 6,550 r.p.m.
gives frequencies 530 and 650 c.p.s.

4th and 5th orders 1st stage root strains at 7,900 r.p.m.
gives frequencies 530 and 650 c.p.s.

9th and 10th orders 4th stage root strains at 4,600 r.p.m.
gives frequencies 670 and 770 c.p.s.

8th and 9th orders 4th stage root strains at 5,000 r.p.m.
gives frequencies 670 and 770 c.p.s.

6th and 7th orders 4th stage root strains at 5,700 r.p.m.
gives frequencies 550 and 670 c.p.s.

The peak differing from the natural frequency of the particular blade was forced due to the resonance of blades in adjacent stages. The peak excited by rotor and stator blade resonances in adjacent rows was of similar amplitude, showing that energy was transferred mainly *via* the air stream rather than *via* coupling through the outer casing.

The frequencies at the peak of the curves are listed below with the blade row having a similar natural frequency.

1*st Stage Pressure Element*

Frequency at peak	410 417 450	500	525 530
	1S	3R	2S

1*st Stage Root Strain-Gauge*

330 367 370		410 417 467		510		525 530		650
1R		1S		3R		2S		4R

4*th Stage Root Strain-Gauge*

530	540	550			670	690			770,	780,	790,	800
	2S					4R			4S		5R	

It will be noted that the transference of energy in the air stream extended 3 stages upstream and 2 stages downstream.

Transference of energy at the natural frequencies of the blading was demonstrated also in the following way. Sound waves were passed through the compressor from a loudspeaker placed in the compressor intake and the variation of sound pressure with frequency measured in one of the fifth-stage bleeds. The measurements were made using a one-half inch diameter tourmaline crystal sandwich as a microphone. Fig. 15 shows the variation of sound pressure with frequency in the bleed, sound pressure in the intake being maintained at a constant level.

The major peaks of the response curve of Fig. 15 are listed in Table 2, some of the peaks occurring at frequencies close to natural frequencies of the blading. Such coincidences are marked against the left-hand column of the table, and in the right-hand column are grouped the corresponding frequencies measured by the strain-gauges during the running of the engine.

5. *Correlation of Data.*—5.1. *Alternating Pressure Readings.*—The results have been expressed as a ratio of the stage pressure rise, which was calculated for the design point (Refs. 1, 2, 3 and 4) and assumed to be proportional to delivery pressure.

The stage pressure rise in Stage 1 was plotted in Fig. 16 and the ratio of the peak oscillating pressures (as measured by the pressure pick-up) due to the various blade resonances divided by the stage pressure rise in Fig. 17. The envelope of these points varied from 5 per cent at full speed to 40 per cent at half speed.

The axial component of thrust is derived in Appendix I. For order m of a stage with N_R rotor blades the thrust acting on a stator blade:

$$t_{m\,s} \propto P_m \sum_{n'=1}^{n'=N_R} \cos m\left(\theta + \frac{2\pi n'}{N_R}\right).$$

The corresponding thrust acting on a rotor blade:

$$t_{m\,R} \propto P_m \sum_{n'=1}^{n'=N_s} \cos m\left(\theta + \frac{2\pi n'}{N_s}\right).$$

Where N_s defines the number of stator blades. In the case of the rth order where r is an integral multiple of the product $(N_s \times N_R)$ these thrusts are directly related such that:

$$tr_R = \frac{N_s}{N_R}\, tr_s \quad (N_s \neq N_R)\,.$$

5.2. *Alternating Stresses.*—Gas bending stresses were calculated for the design point (Ref. 3) using the expression:

Gas bending stress

$$q = \Lambda\sigma \frac{S}{C_{m/d}} \cdot \frac{C_{m/d}}{C_{\text{ROOT}}} \cdot \frac{\Delta T_S}{10}\left(\frac{h_0}{C_{\text{ROOT}}}\right)^2\left(\frac{1}{10\ t/C_{\text{ROOT}}}\right)^2 \text{ tons/sq in.}$$

where Λ is a factor depending on $\dfrac{U}{V_{a\,m/d}}$

σ	is	relative density
S		blade pitch
C		blade chord
h_0		blade height
ΔT_S		stage temperature rise

The assumption was made that the gas bending stresses varied as the square of the compressor speed. These were calculated at the root section and at a section 0·375 in. from the root for the first- and fourth-stage stator blades and are shown plotted in Fig. 18.

The alternating blade stress at resonance was divided by the corresponding gas bending stress and plotted in Fig. 19, the envelope having values of 0·6, 1·3, and 2, at compressor speeds of 8,000, 6,000 and 4,000 r.p.m. respectively.

The ratio of the sum of the harmonic components of alternating stress to the corresponding gas bending stress was plotted in Fig. 20. The envelope varied from 0·6 at 8,000 r.p.m. to 3·7 at 4,000 r.p.m.

5.3. *Blade Damping.*—An estimate of the overall damping present was obtained by calculating the input energies and maximum kinetic energies for the first-stage stator blade vibrating in the fundamental flexural mode. These quantities were then related by employing the observed values of alternating pressure and stress.

5.3.1. *Calculation of kinetic energy.*—The deflection curve of a first-stage stator blade was obtained by vibrating it in the fundamental flexural mode (Fig. 21). From this curve and a knowledge of blade scantlings the bending moment was determined for an arbitrary tip deflection. The bending moment and maximum kinetic energy at the strain-gauge location has been derived for a tip deflection of one inch in Table 3. The tip deflections corresponding to the measured stresses at fundamental or near fundamental resonances are given in Table 5.

5.3.2. *Estimation of input energy.*—Expression of the input energy in terms of the pressure element readings required a knowledge of the pressure distribution around the aerofoil section and along the blade.

Pressure distributions around the sections were obtained from cascade data (Ref. 2) and the sections approximating most nearly in aerodynamic performance to those used in the compressor were aerofoil sections 11C2/33P40 and 10C1/40C50 respectively (Figs. 22 and 23). The assumption was made that the alternating pressure distribution acting on a section was similar to the steady distribution.

Summation of the pressure around these aerofoil sections (with due regard to sign) gave the following factors for the ratio $\frac{\text{mean pressure on the section}}{\text{pressure measured by element}}$:

11C2/33P40		10C1/40C50	
Theoretical	Experimental	Theoretical	Experimental
1·64	2·34	2·34	2·43

A value for this factor of 2·4 was used in the remainder of the calculations.

Variations of pressure along the blade was determined as follows:

Assuming vortex flow between the first-stage rotor blade and the first-stage stator blade, and between the first-stage stator blade and second-stage rotor blade, the equation for radial equilibrium was applied, *viz.*:

$$\frac{1}{\rho}\frac{dp}{dr} = \frac{Vw^2}{r}$$

where

ρ is fluid density
P fluid pressure
Vw velocity of whirl

hence

$$\dot{p} = \Sigma\rho \frac{Vw^2}{r} \delta r .$$

Assuming mean stage pressures at mean diameter, and employing graphical integration of values obtained from the velocity triangles, the pressures before and after the first-stage stator blade were calculated for points along its length, and hence the mean pressure acting on the blade was obtained (Fig. 24).

Input energies to the blade were calculated at each section for unit alternating pressure at the measuring element employing the values of pressure distribution around the blade and along its length obtained above, and are given in Table 4. The total input energies for the pressures measured at the blade resonances are given in Table 5 and were found to be high relative to the estimated maximum kinetic energies.

A number of experiments was made in the laboratory to estimate the effects of material and blade-root damping.

This showed that contributory factors to this high damping were:

(*a*) Light blade-root platform

(*b*) Loose fit of some blades.

In all cases the value of damping changed with blade amplitude. Addition of a pressure measuring element increased the damping and addition of the strain-gauges caused a slight increase in damping over a standard blade.

Conclusions.—Analysis of the oscillating pressure and strain readings showed that the excitation could be grouped as follows:

Source of excitation	Alternating pressure 1st stage	Alternating strain			
		1st stage		4th stage	
		Root	Tip	Root	Tip
1. Non-uniform entry	1, 2, 4, 5, 6, 7, 8, 18	3, 4, 5, 6, 7, 8	1, 2, 6	6, 7, 8, 9, 10	1, 2, 4, 7, 8, 9
2. Intake spider	33, 44, 77, 88	22	22	11	11, 44
3. Rotor blades passing stator blades	36, 72, 108, 144, 180, 216, 252	36, 72	36, 72	36, 72	36, 72

The higher orders predominated at the lower compressor speeds and airflows, indicating irregular airflow under these conditions.

Analyses of the strain-gauge records were of similar form to the above, but limited to the lower orders indicating that the blades were more responsive to the lower frequency excitations.

The curves of oscillating pressure had peak values for the natural frequency of the blades in a stage and of the blades in adjacent stages.

Resonance of blades, particularly in the fundamental flexural mode set up fluctuations in the air stream at that frequency and caused transference of energy between stages. Due to the geometry of the compressor, orders in Groups 1 and 2 when summated will be zero and initial impulses of them will not be sustained except due to lack of symmetry or through disturbance in the flow. Orders listed in Group 3 are in phase when summated and may be sustained in the compressor, but orders in this category which should in theory summate to zero or produce forward or reverse couples were not detected. The compressor used for this investigation had the same number of rotor blades and the same number of stator blades in the first five stages, but if these had been different summation around the annulus would have eliminated some orders by reducing the transference.

Alternating pressure at the various peaks plotted as a percentage of the stage pressure rise varied from 5 per cent at full speed to 40 per cent at half speed.

The ratio of the major harmonic components of the alternating stress at the various peaks to gas bending stress had values of 0·6:1·3:2 at compressor speeds of 8,000, 6,000 and 4,000 r.p.m. respectively. The maximum deflection of the first-stage stator blade due to alternating forces was found to be 0·012 in. Calculation of input energies and maximum kinetic energies at resonance for the fundamental or near-fundamental modes showed that the overall blade damping was high. This was caused by the light design of blade-root platform, and loose fit on assembly in the compressor. Although gas bending loads would tend to stiffen the fixing under running conditions, lack of centrifugal loading present in a comparable rotor blade would result in relatively higher damping. The prominence of blade vibration resulting from modulation of the air stream by the vibration of blades in adjacent stages is attributed to this high damping.

REFERENCES

No.	*Author*	*Title, etc.*
1	A. R. Howell	The present basis of axial flow compressor design. Part I: Cascade theory and performance. Part II: Compressor theory and performance. R. & M. 2095. June, 1942.
2	A. D. S. Carter and Hazel P. Hughes ..	A theoretical investigation into the effect of profile shape on the performance of aerofoils in cascade. R. & M. 2384. March, 1946.
3	D. G. Ainley	Estimation of the stresses in an axial flow compressor blade. N.G.T.E. Memo. M.55. (Unpublished.) A.R.C. 12,620.
4	F. Poselthwaite, B. C. Carter, W. G. A. Perring and K. V. Diprose.	Vibration of propellers due to aerodynamic forces. Part I: Permissible proximity of a propeller to the leading edge of a wing, as decided by propeller blade vibration.
	J. R. Forshaw, H. B. Squire and F. J. Bigg.	Part II: Vibration of propellers due to non-uniform inflow. R. & M. 2054. April, 1942.

TABLE 1

Natural Frequencies of I.G.V. and First Four Compressor Stages

	I.G.V.	1R	1S	2R	2S	3R	3S	4R	4S	5R
Fundamental flexure	273	377	446	436	530	511	617	626	752	786
1st overtone flexure	1400	1558	2186	1837		2231		2663		3253
2nd overtone flexure	3700	4230		4926		5980		7081		8455
3rd overtone flexure	6800	7715		9364						
Fundamental torsion	1953	2396	2460	2590	2816	2864	2960	3227	3399	3794
1st overtone torsion	4920	5740	6136	6277		7080		8055		

TABLE 2

Resonances Indicated by Loudspeaker and Crystal Microphone

Resonances detected by crystal pick-up in 5th-stage bleed		Resonances extracted from strain-gauge analyses	
80	c.p.s.		
100			
126			
230	I.G.V.		
380	1R	330, 367, 370	1R
		410, 417	1S
510	3R	510	3R
		525, 530, 540, 550	2S
660	4R	650, 670, 690	4R
900			
990			
1100			
1120			
1200			
1350			
1650			
1820			
2000			
2500			
2900			
3400			

TABLE 3

Calculation of Bending Moment and Kinetic Energy for 1-in. Tip Deflection

Blade length at inter-sections L (in.)	Length at mid-section (in.)	Length of section δL (in.)	Area of section (sq in.)	Angle between direction of motion and principal axes of base section (deg)	Deflection relative to tip Z_1	Z_1^2	Distance of c.g. of section from base section L_1	B.M./ω^2 = $2{\cdot}72 \cdot 10^{-4}$ Area $\delta L \cdot L_1 \cdot Z_1$ (lb in. sec^2)	K.E./ω^2 = $2{\cdot}72 \cdot 10^{-4}$ Area $\cdot \delta L \cdot Z_1^2$ (lb in. sec^2)
3·902									
	3·822	0·060	0·088	88·3	1	1	3·447	$0{\cdot}049 \times 10^{-4}$	$0{\cdot}0144 \times 10^{-4}$
3·782									
	3·641	0·282	0·092		0·920	0·848	3·266	$0{\cdot}212 \times 10^{-4}$	$0{\cdot}0597 \times 10^{-4}$
3·5									
	3·375	0·25	0·099		0·816	0·668	3	$0{\cdot}166 \times 10^{-4}$	$0{\cdot}0450 \times 10^{-4}$
3·25									
	3·125	0·25	0·105		0·726	0·528	2·75	$0{\cdot}143 \times 10^{-4}$	$0{\cdot}0378 \times 10^{-4}$
3									
	2·875	0·25	0·112		0·611	0·374	2·5	$0{\cdot}117 \times 10^{-4}$	$0{\cdot}0285 \times 10^{-4}$
2·75									
	2·625	0·25	0·118		0·522	0·273	2·25	$0{\cdot}094 \times 10^{-4}$	$0{\cdot}0219 \times 10^{-4}$
2·5									
	2·375	0·25	0·125		0·428	0·184	2	$0{\cdot}073 \times 10^{-4}$	$0{\cdot}0156 \times 10^{-4}$
2·25									
	2·125	0·25	0·132		0·335	0·112	1·75	$0{\cdot}053 \times 10^{-4}$	$0{\cdot}0101 \times 10^{-4}$
2									
	1·875	0·25	0·138		0·266	0·071	1·5	$0{\cdot}037 \times 10^{-4}$	$0{\cdot}0067 \times 10^{-4}$
1·75									
	1·625	0·25	0·144		0·204	0·042	1·25	$0{\cdot}025 \times 10^{-4}$	$0{\cdot}0041 \times 10^{-4}$
1·5									
	1·375	0·25	0·151		0·143	0·021	1	$0{\cdot}015 \times 10^{-4}$	$0{\cdot}0021 \times 10^{-4}$
1·25									
	1·125	0·25	0·158		0·094	0·009	0·75	$0{\cdot}008 \times 10^{-4}$	$0{\cdot}0009 \times 10^{-4}$
1									
	0·875	0·25	0·165		0·057	0·003	0·5	$0{\cdot}003 \times 10^{-4}$	$0{\cdot}0004 \times 10^{-4}$
0·75									
	0·625	0·25	0·172		0·025	0·001	0·25	$0{\cdot}001 \times 10^{-4}$	$0{\cdot}0001 \times 10^{-4}$
0·5									
	0·375	0·25	0·178		0·012		0	0	
0·25									
	0·125	0·25	0·185		0·004				0
0									
For blade material:— $\frac{\rho}{g} = \frac{0{\cdot}105}{386} = 2{\cdot}72 \times 10^{-4}$ lb in.$^{-4}$ sec^2								$0{\cdot}996 \times 10^{-4}$	$0{\cdot}2473 \times 10^{-4}$

TABLE 4

Calculation of Energy Input per Cycle for Unit Pressure at Element

L (in.)	δL (in.)	Z_1	Chord C (in.)	Section pressure relative to pressure at element $\frac{P}{P_{0\cdot85}}$	Input energy cycle $= 2\cdot4\,\frac{P}{P_{0\cdot85}}\,.\,C\,.\,\delta L\,.\,\pi\,.\,Z_1$ (lb/in.)
3·902					
	0·060	1	1·265	0·87	0·498
3·782					
	0·282	0·920		0·91	2·250
3·5					
	0·25	0·816		0·98	2·000
3·25					
	0·25	0·726		1·03	1·780
3					
	0·25	0·611		1·07	1·562
2·75					
	0·25	0·522		1·13	1·405
2·5					
	0·25	0·428		1·17	1·190
2·25					
	0·25	0·335		1·21	0·966
2					
	0·25	0·266		1·25	0·792
1·75					
	0·25	0·204		1·28	0·624
1·5					
	0·25	0·143		1·31	0·446
1·25					
	0·25	0·094		1·33	0·298
1					
	0·25	0·057		1·37	0·186
0·75					
	0·25	0·025		1·39	0·081
0·5					
	0·25	0·012		1·42	0·041
0·25					
	0·25	0·004		1·44	0·014
0					
					14·133

TABLE 5

Energy Relations for Modes in Compressor

Frequency (c.p.s.)	$\omega^2 \div 10^6$	Order	Speed (r.p.m)	Alternating stress ($\pm$ lb/sq in.)	Alternating pressure ($\pm$ lb/sq in.)	Stress for 1-in. tip deflection (lb/sq in.)	Tip deflection Z_{TIP} ($\pm$ in.)	Frequency (c.p.s.)	Energy input/cycle $\delta W = \left(\Sigma 9{\cdot}54 \frac{P}{P_{0{\cdot}85}} . \delta L . Z_1\right) \times (P_{0{\cdot}85} . Z_{TIP})$	Maximum kinetic energy $2W = (\Sigma 2{\cdot}72 . 10^{-4} . \text{Area} . \delta L . Z_1^2) \times (Z_{TIP}^2 . \omega^2)$
467	8·60	4	7020	2150	0·042	182,800	0·012	467	0·007	0·029
467	8·60	8	3510	550	0·025	182,800	0·003	467	0·001	0·002
410	6·63	6	4100	920	0·081	172,000	0·005	410	0·006	0·005
417	6·86	5	5020	1220	0·118	146,000	0·008	417	0·014	0·012
510	10·12	6	5100	1860	0·071	215,000	0·009	510	0·009	0·019
530	11·10	4	7950	1460	0·044	236,000	0·006	530	0·004	0·011

APPENDIX I

Derivation of Relation Between Pressure on a Blade Section and the Pressure in the Compressor Annulus

If P_1, V_1, denote upstream conditions

P_2, V_2, denote downstream conditions

w denote losses in cascade

$$\Delta P = P_2 - P_1$$

$$= \tfrac{1}{2}\rho(V_2^2 - V_1^2) - w .$$

If the sections are taken across a cascade where:

V_A is axial velocity

α_1 inlet air angle

α_2 outlet air angle ,

for a design based on constant axial velocity:

$$\Delta P = \tfrac{1}{2}\rho V_A^2(\tan^2 \alpha_1 - \tan^2 \alpha_2) .$$

The force acting on δr width of annulus:

$$= s\, \delta r\, \Delta P .$$

The force acting on length δr of blade section:

$$= c\, \delta r\, \Delta p$$

where Δp is the mean pressure over the section.

Hence $s\, \delta r\, \Delta P = c\, \delta r\, \Delta p$.

Therefore $\Delta P = \frac{c}{s}\Delta p$.

Taking the oscillating components of pressure and neglecting phase angles:

$$\Delta p = p_0 + p_1 \cos\theta + p_2 \cos 2\theta + \ldots\ldots\ldots + p_n \cos n\theta$$

and

$$\Delta P = \frac{c}{s}[p_0 + p_1 \cos\theta + p_2 \cos 2\theta + \ldots\ldots\ldots + p_n \cos n\theta] .$$

The axial component of thrust for order m of a stage with N rotor blades is

$$\propto \frac{c}{s} p_m \sum_{n_1=1}^{n_1=N} \cos m\left(\theta + \frac{2\pi n'}{N}\right) .$$

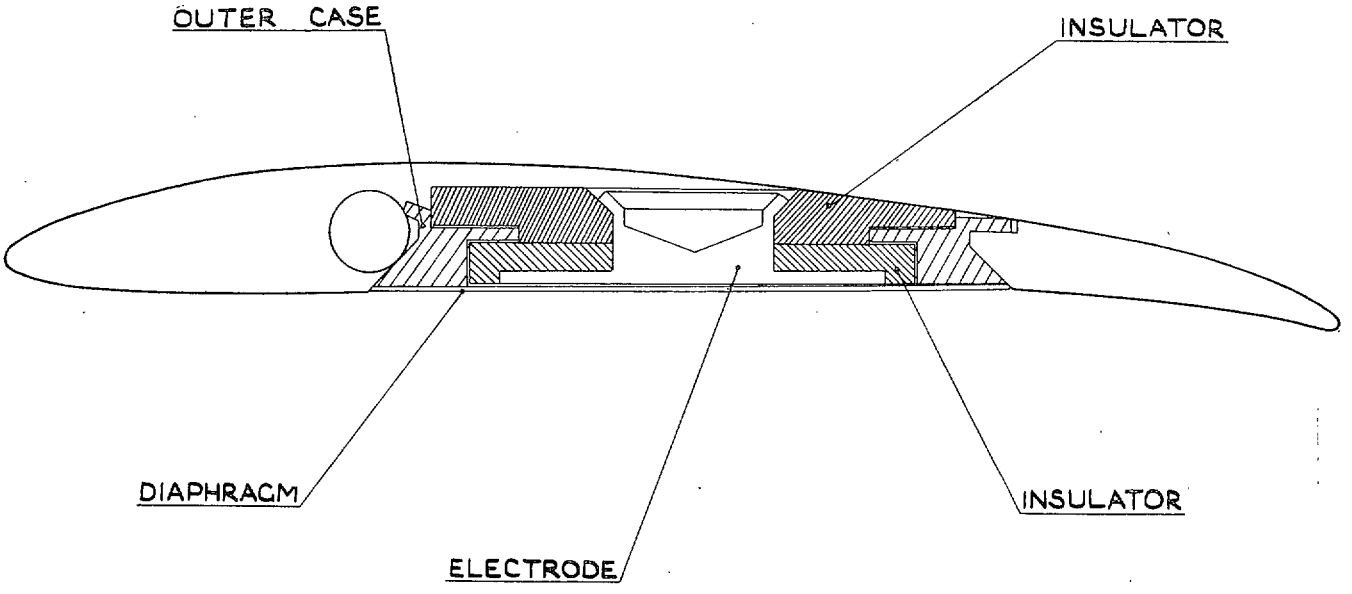

FIG. 1. Section through blade and pressure element (preliminary design).

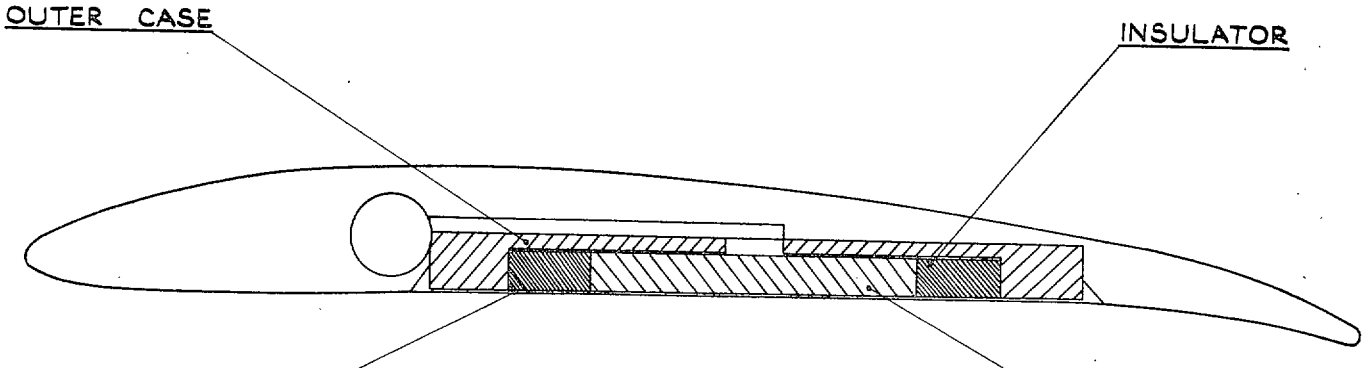

FIG. 2. Section through blade and pressure element used in experiments.

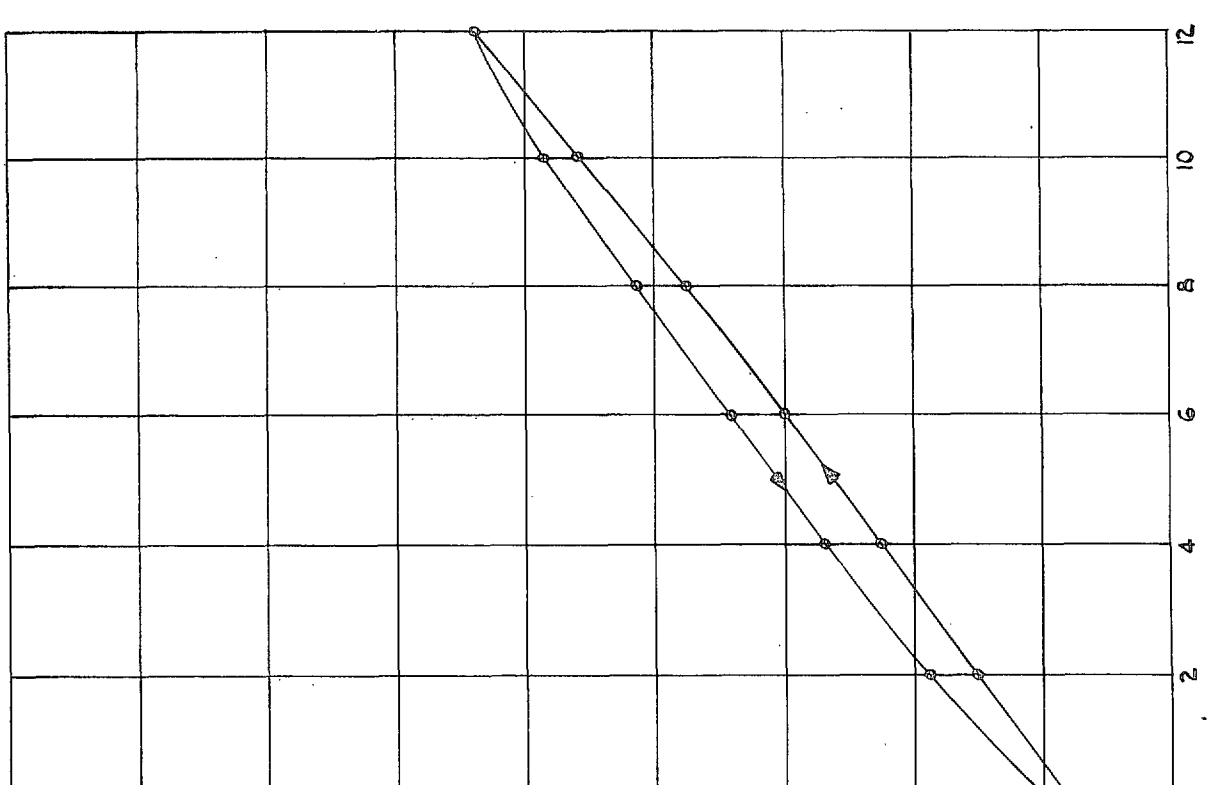

FIG. 3. Typical calibration curve of pressure element installed in compressor blade.

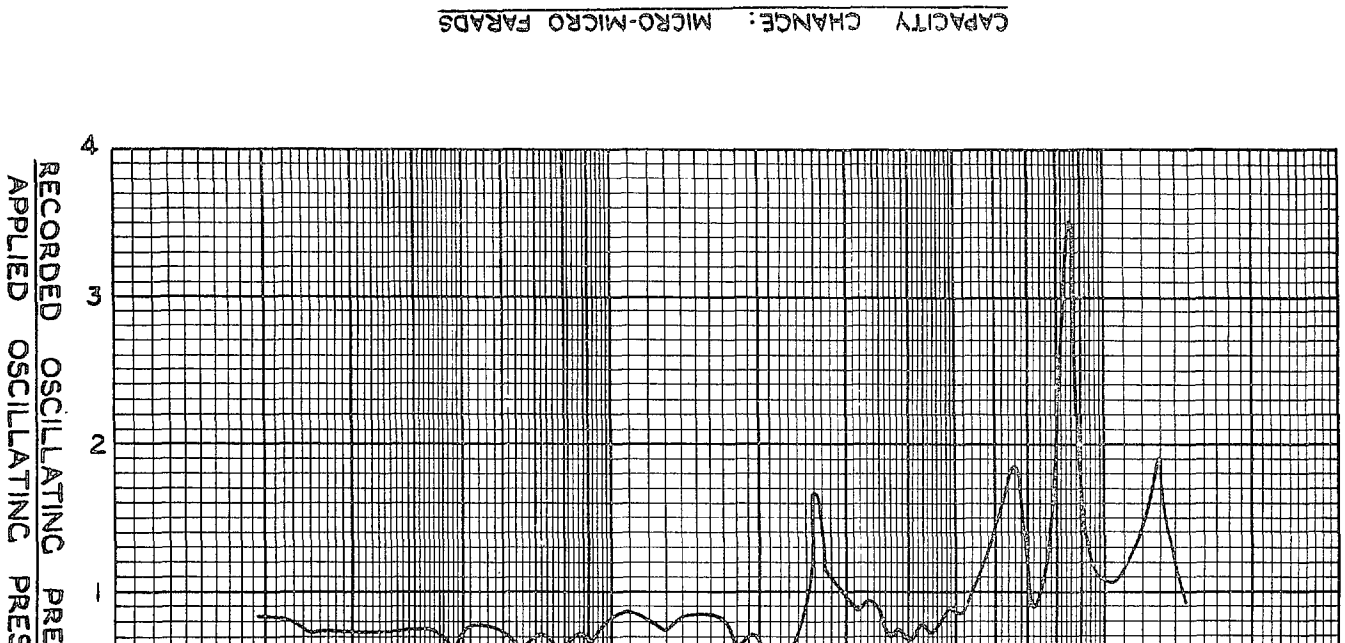

FIG. 4. Calibration curve of pressure element in first-stage stator.

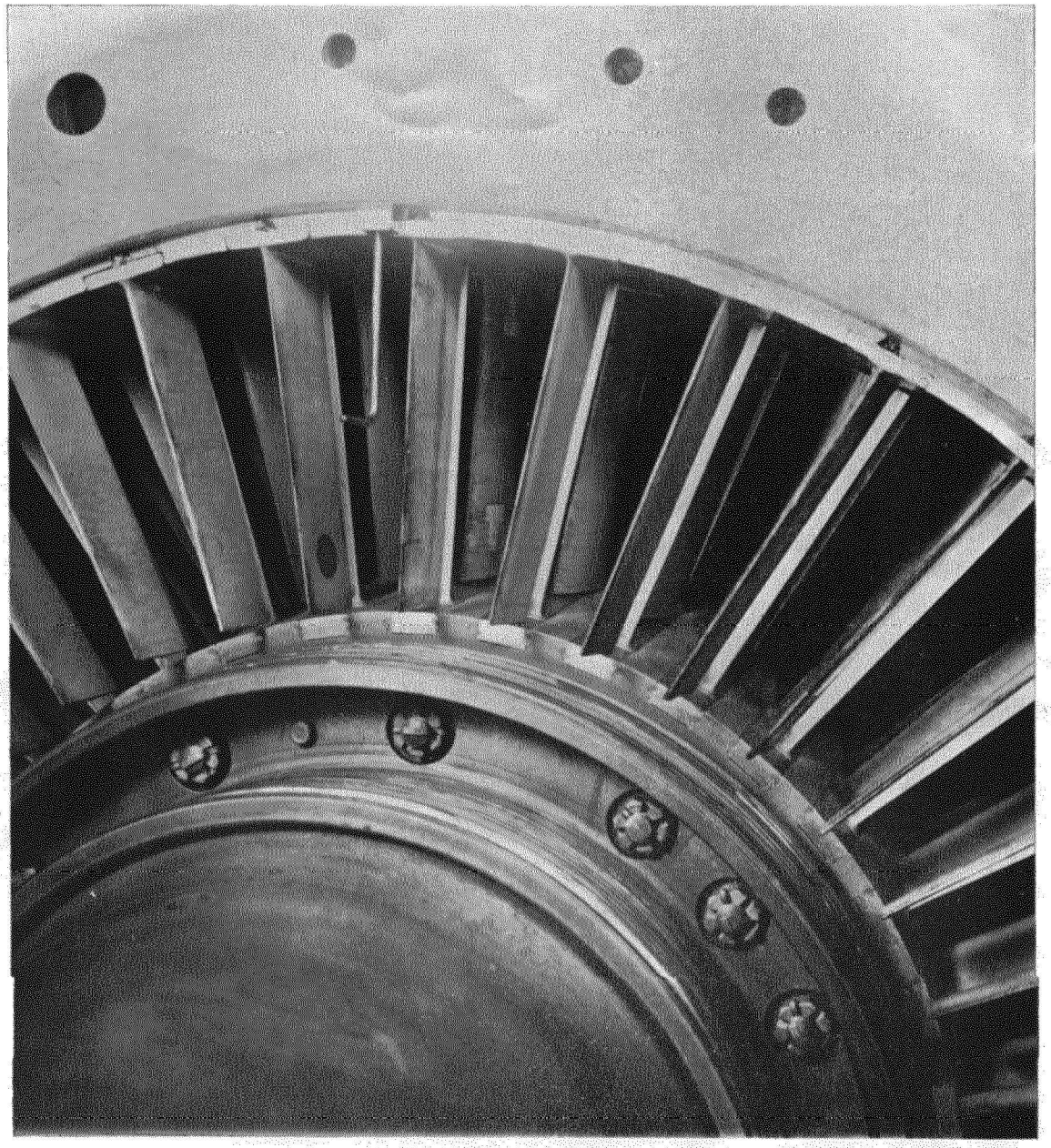

FIG. 5. Pressure element, wire strain-gauge, etc., installed in compressor.

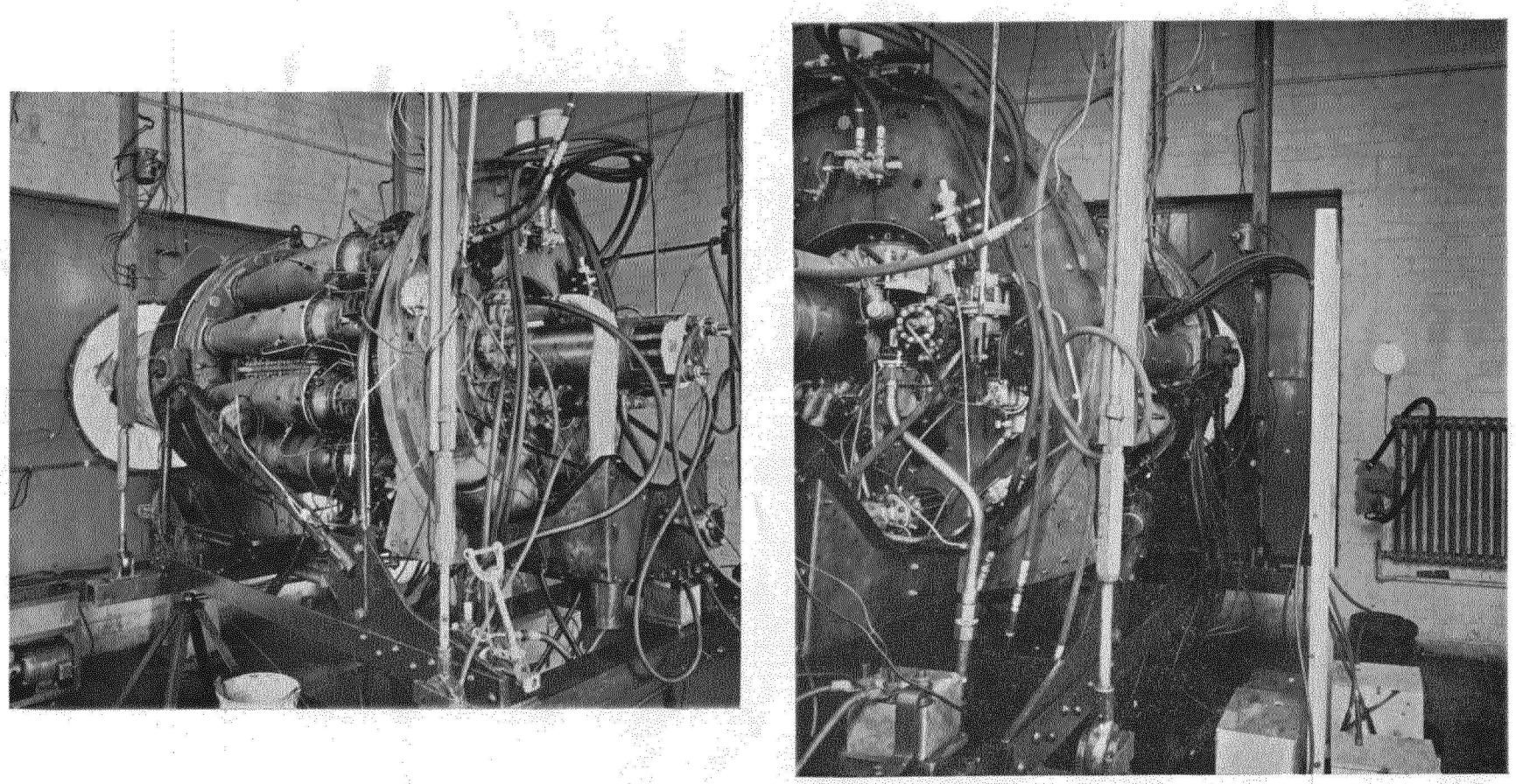

FIG. 6. Engine in test cell.

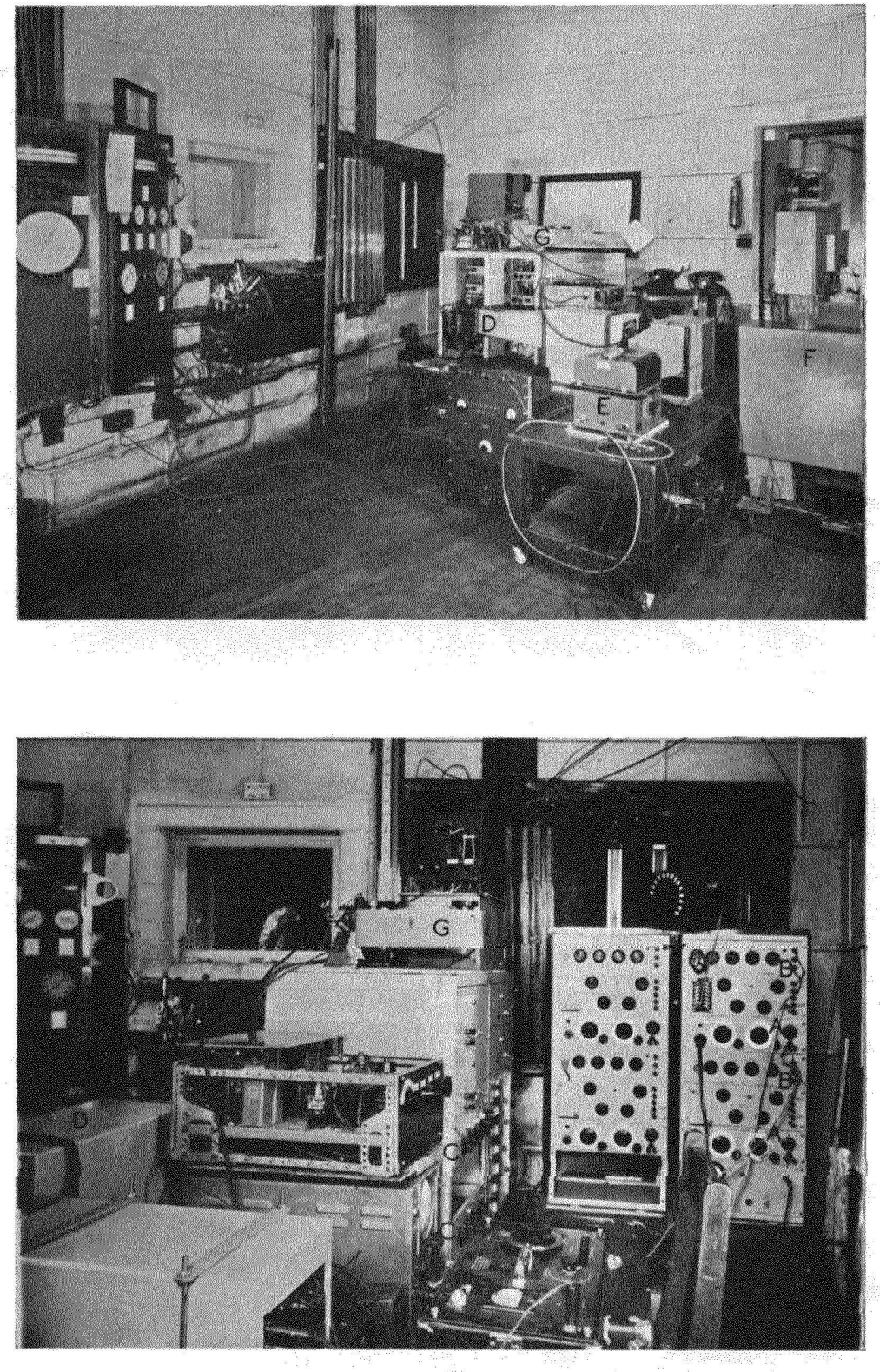

FIG. 7. Electronic equipment in observation room.

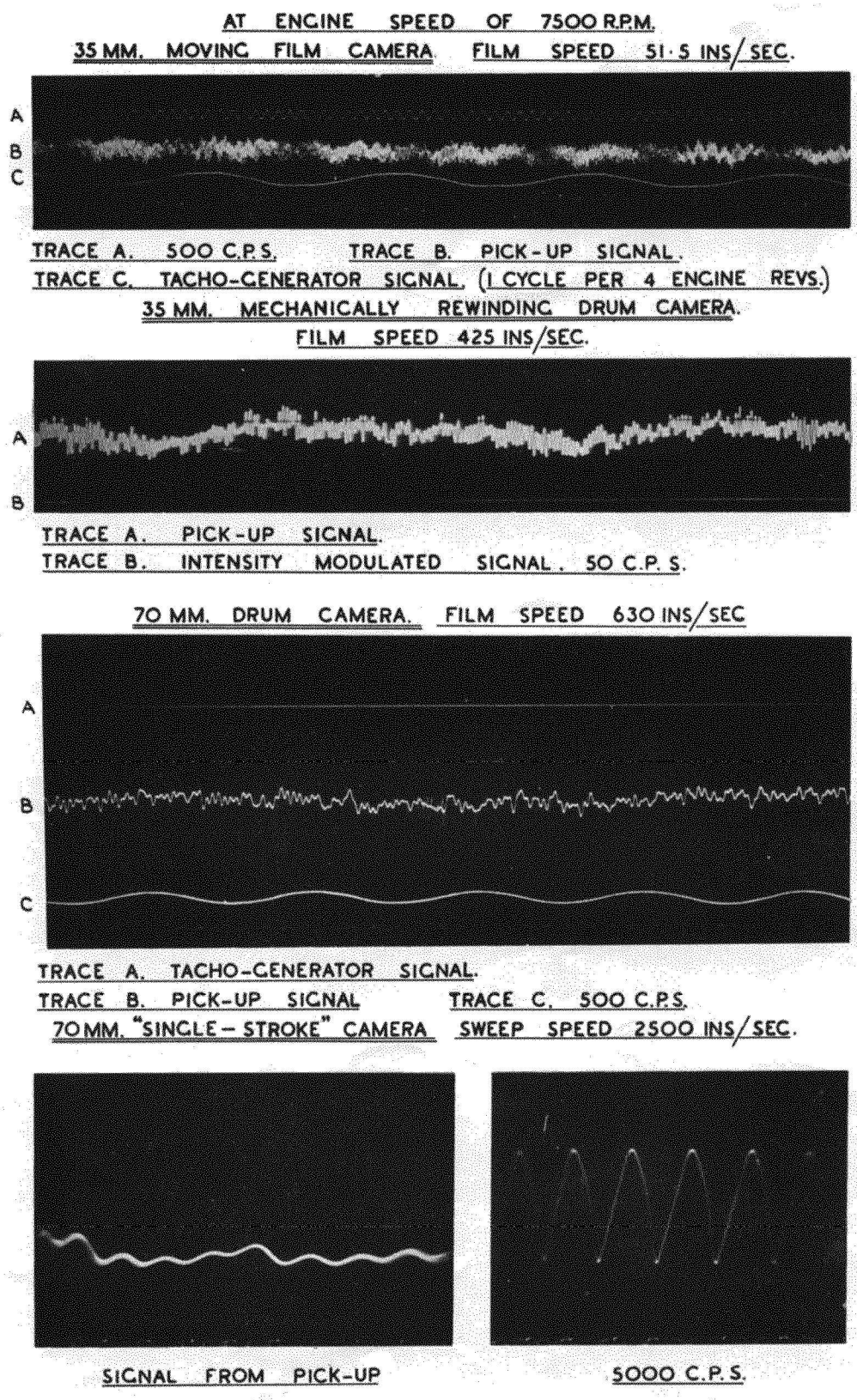

FIG. 8. Records of alternating aerodynamic pressures.

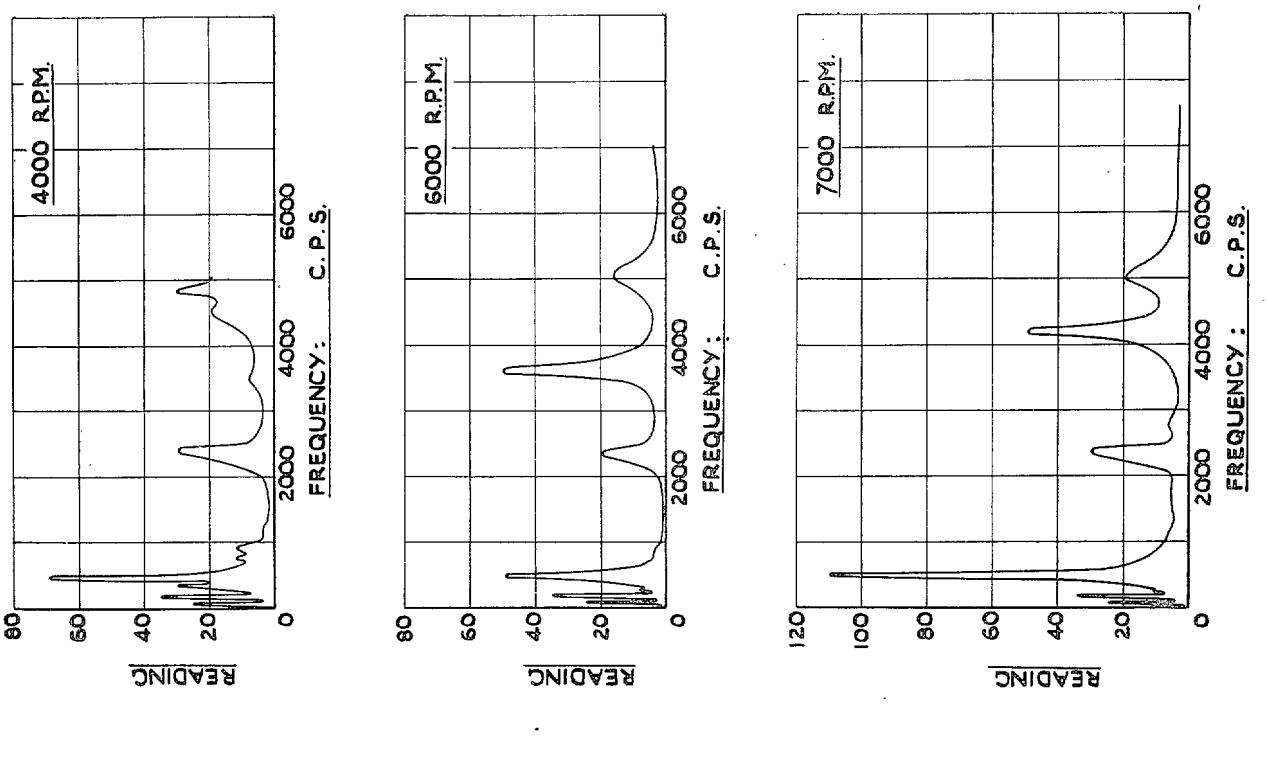

FIG. 9. Harmonic analysis by G.R. analyser of signal from first-stage stator-pressure element.

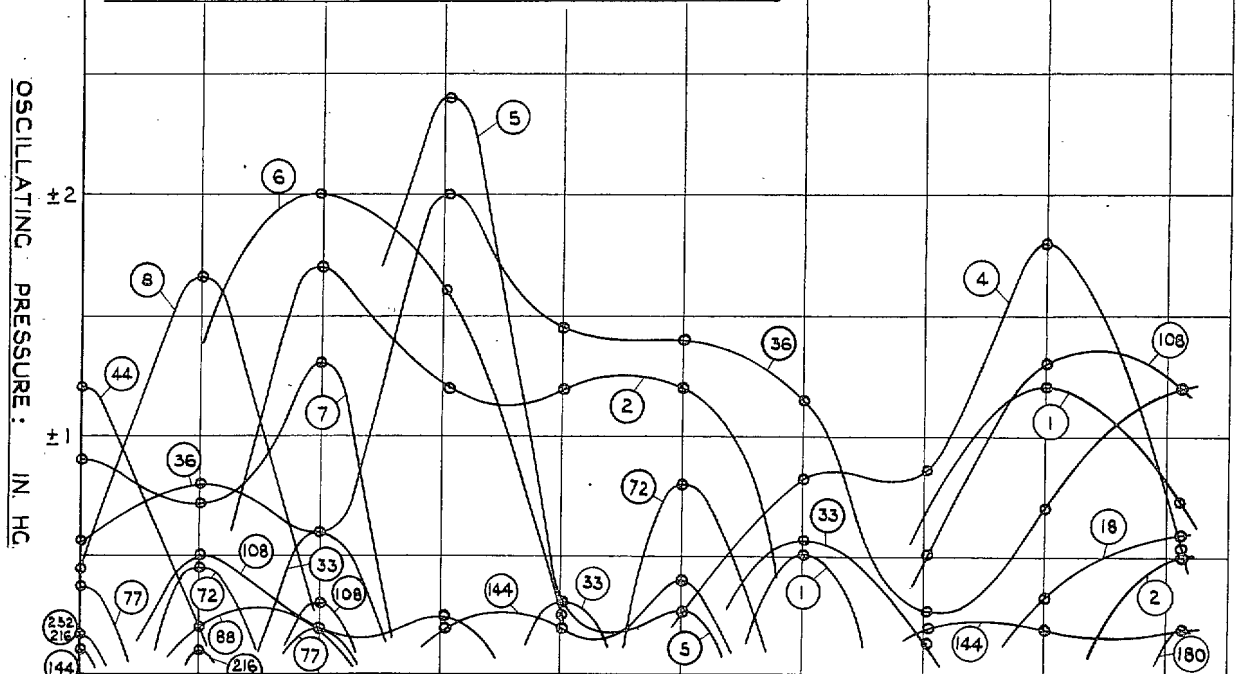

FIG. 10. Predominant harmonic components of oscillating pressure for first-stage stator blade.

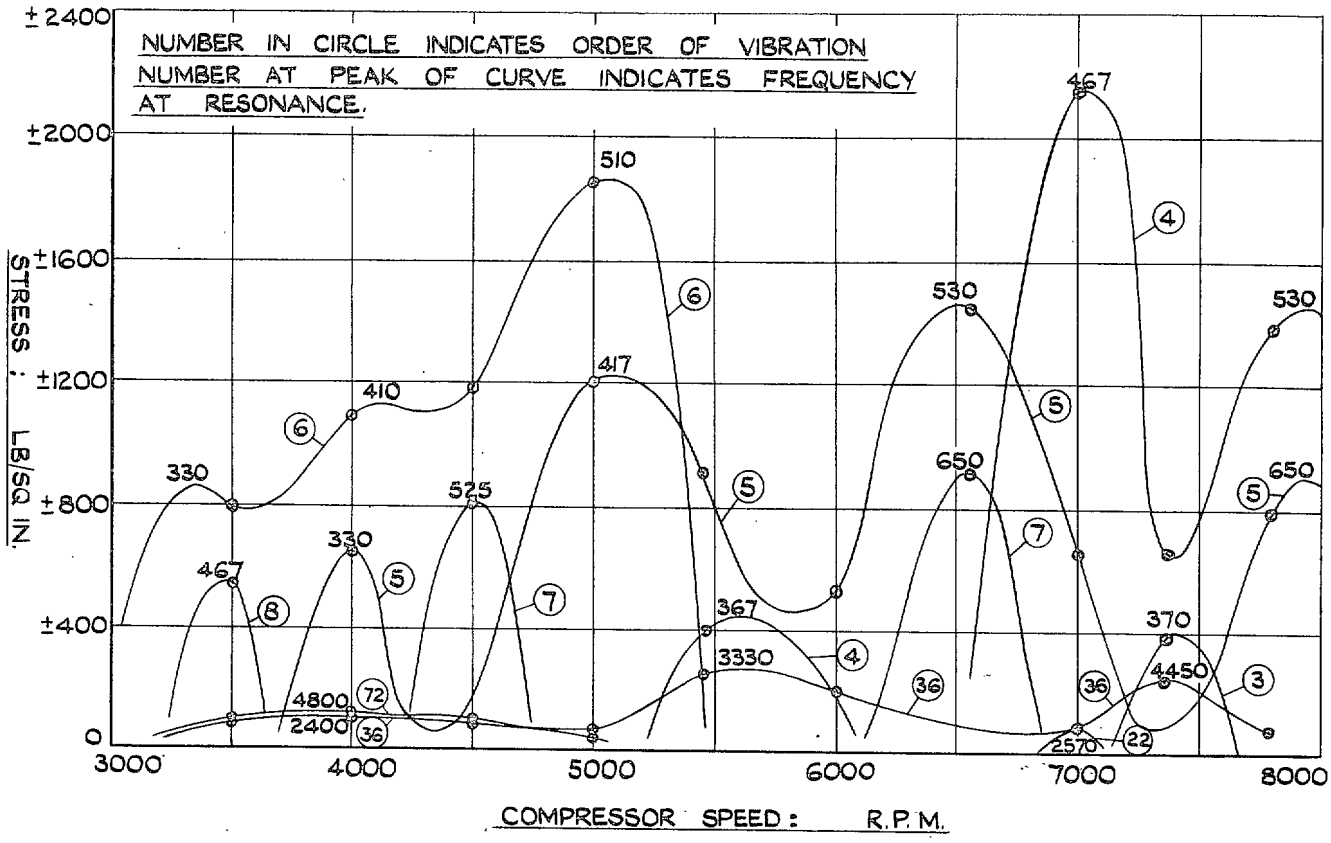

FIG. 11. Predominant harmonic components of stress at root of first-stage stator blade.

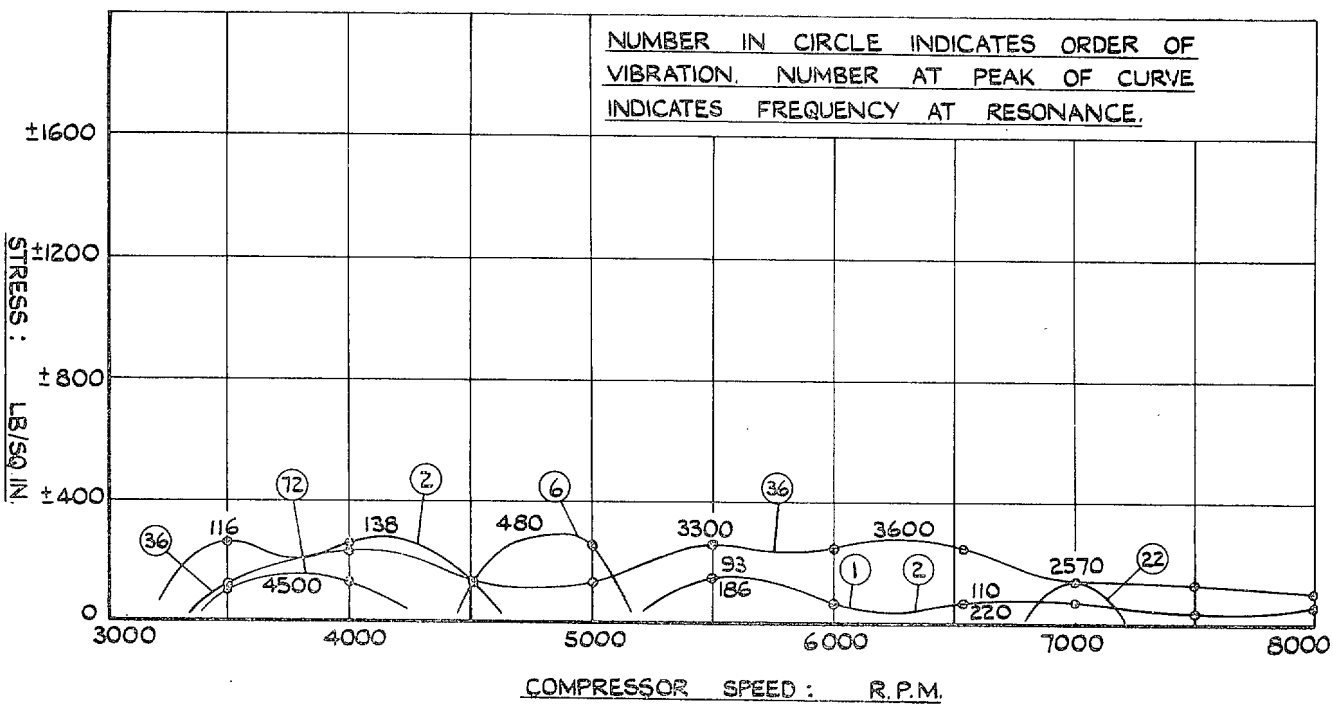

FIG. 12. Predominant harmonic components of stress at 0·85 length of first-stage stator blade.

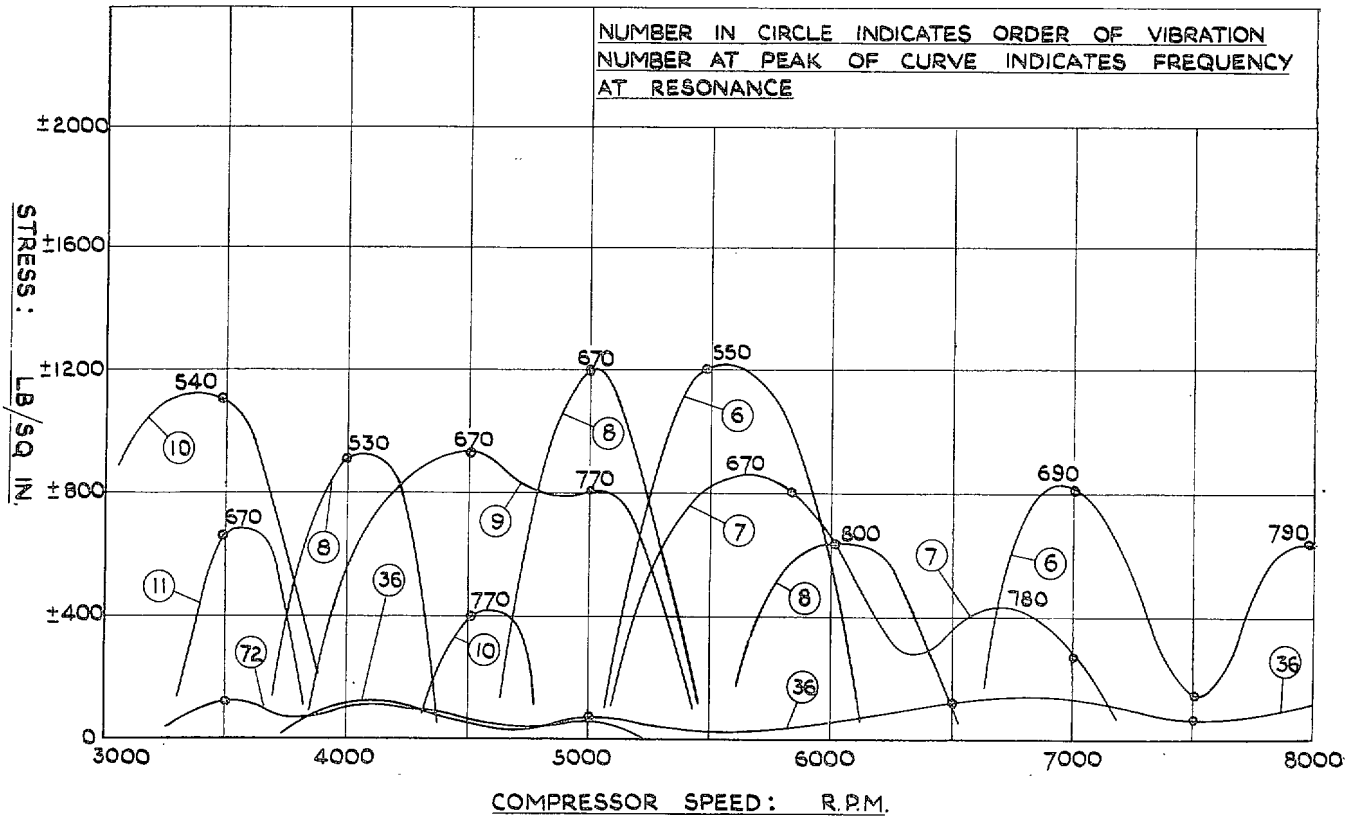

FIG. 13. Predominant harmonic components of stress at root of fourth-stage stator blade.

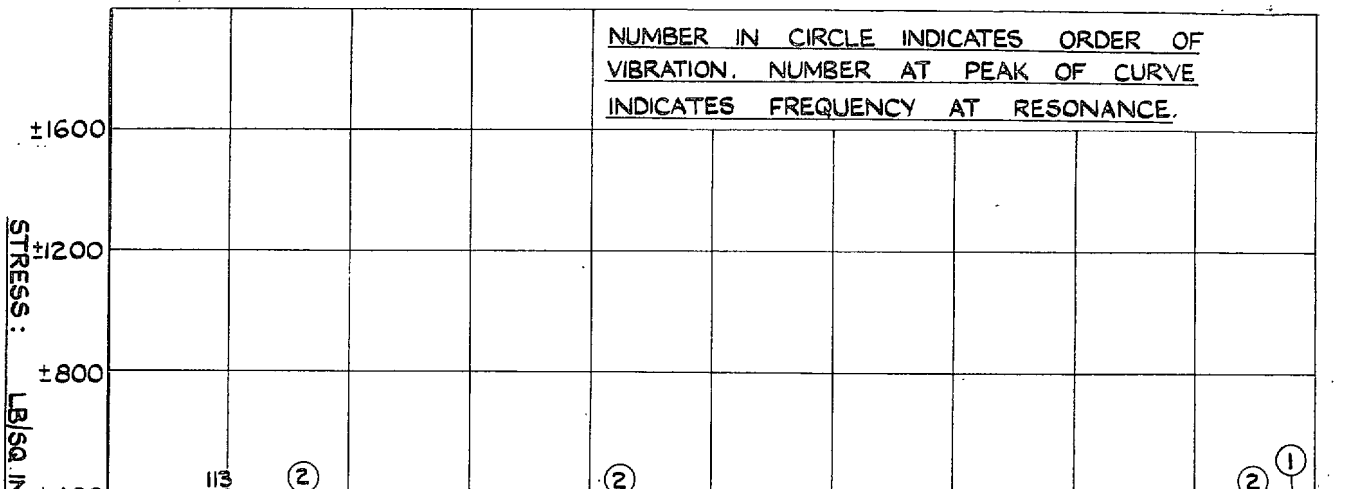

FIG. 14. Predominant harmonic components of stress at 0·85 length of fourth-stage stator blade.

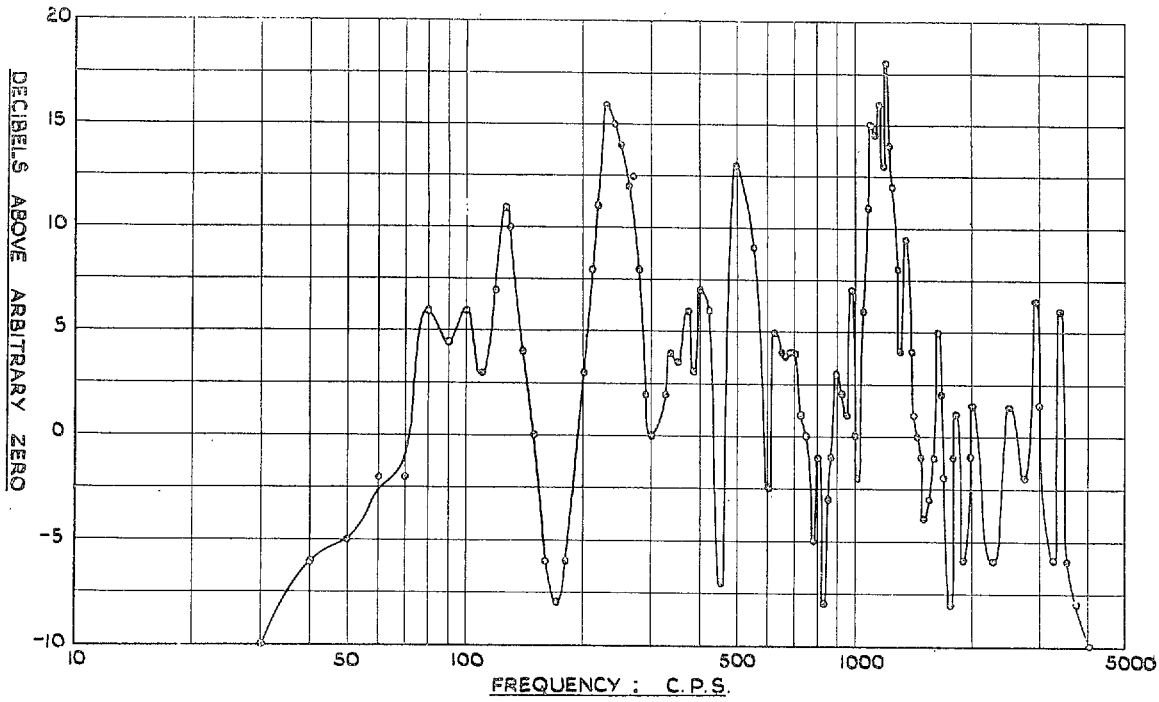

FIG. 15. Output from crystal pick-up placed in fifth-stage bleed and excited by loudspeaker placed in inlet.

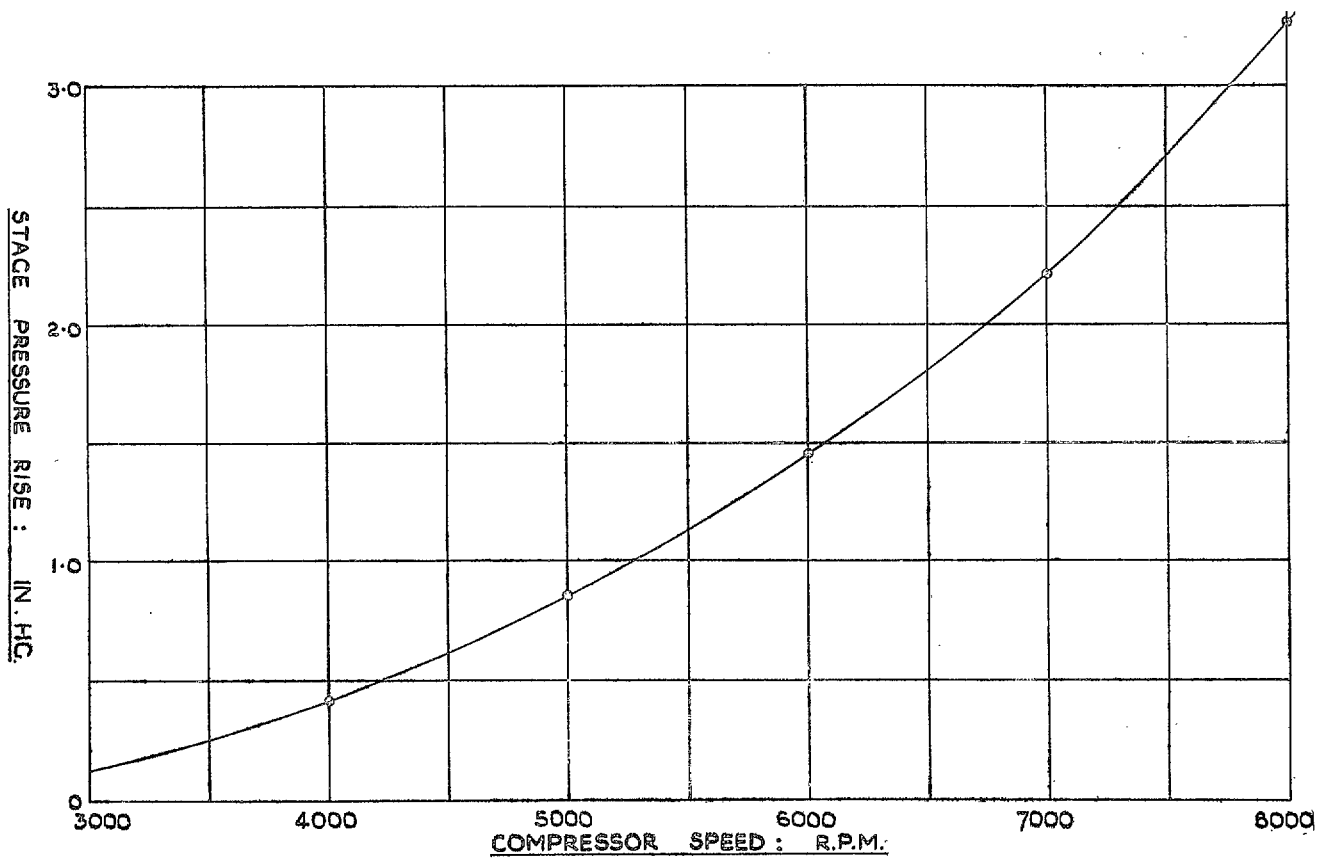

FIG. 16. First-stage pressure rise.

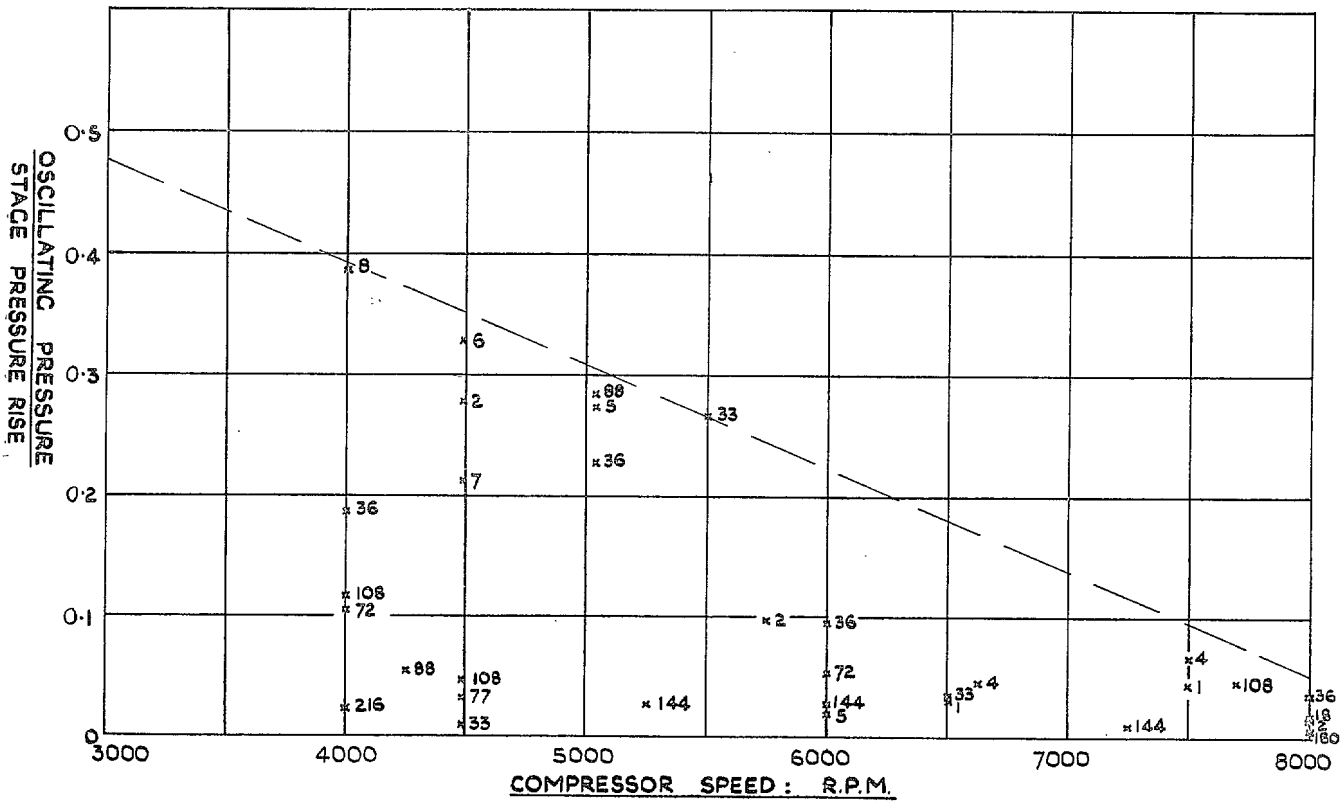

FIG. 17. Ratio of oscillating pressure to stage pressure rise for first stage.

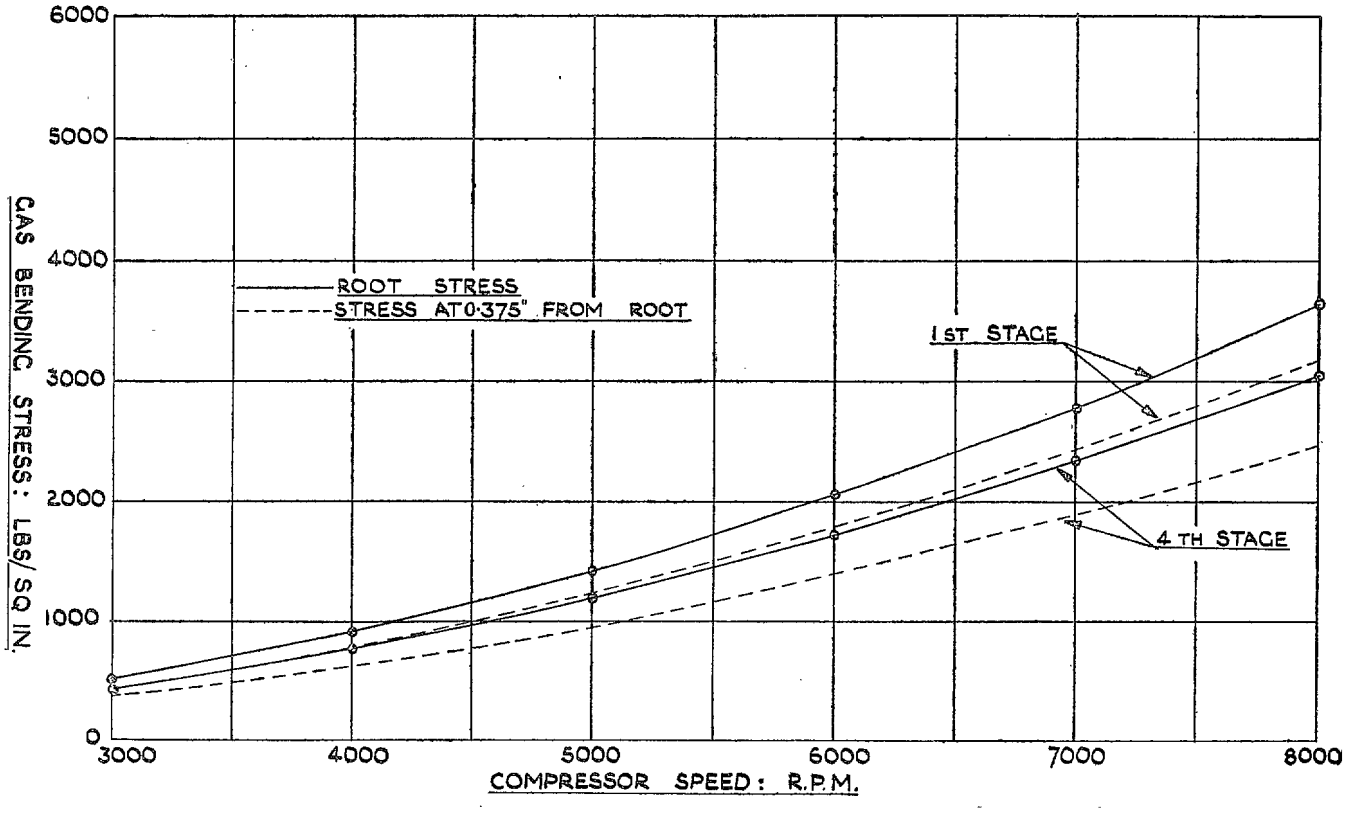

FIG. 18. Gas bending-stresses.

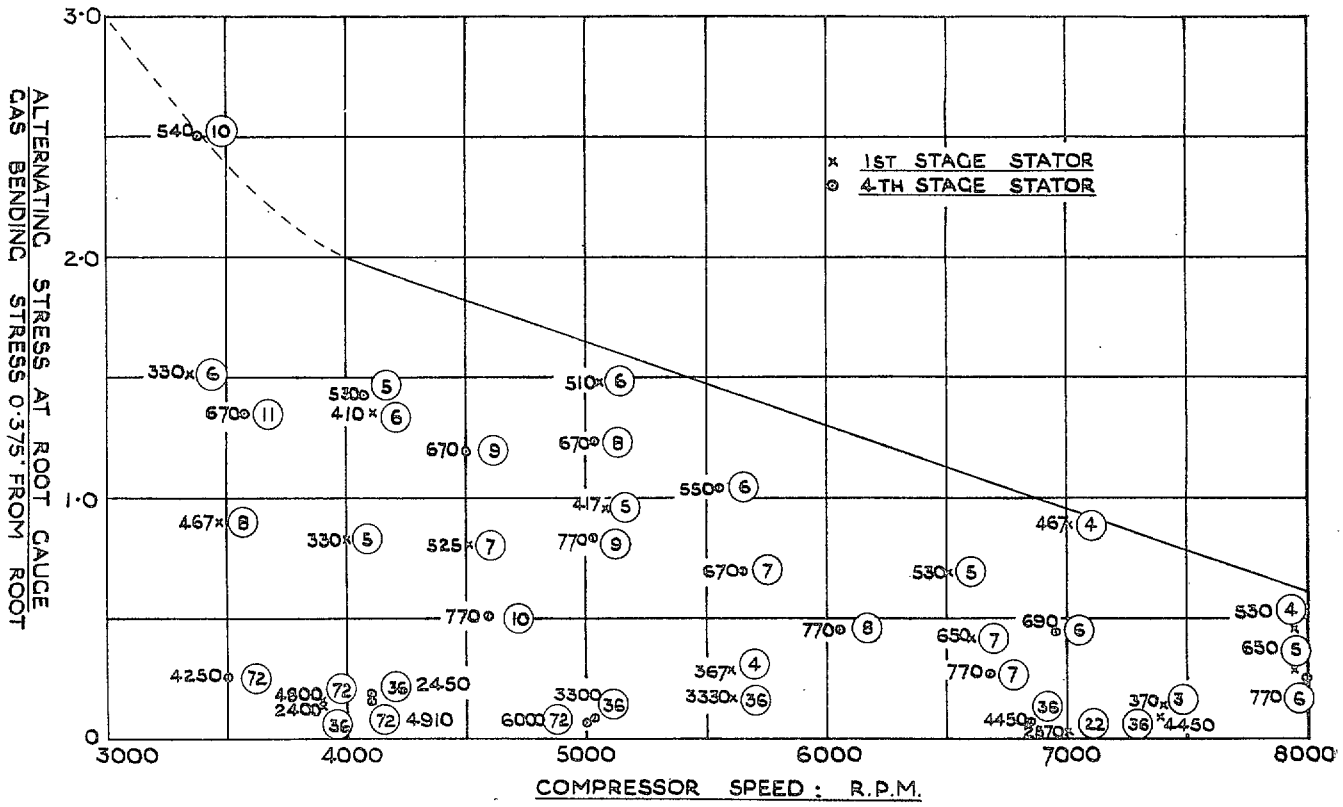

FIG. 19. Ratio of harmonic components of alternating stresses to gas bending-stresses.

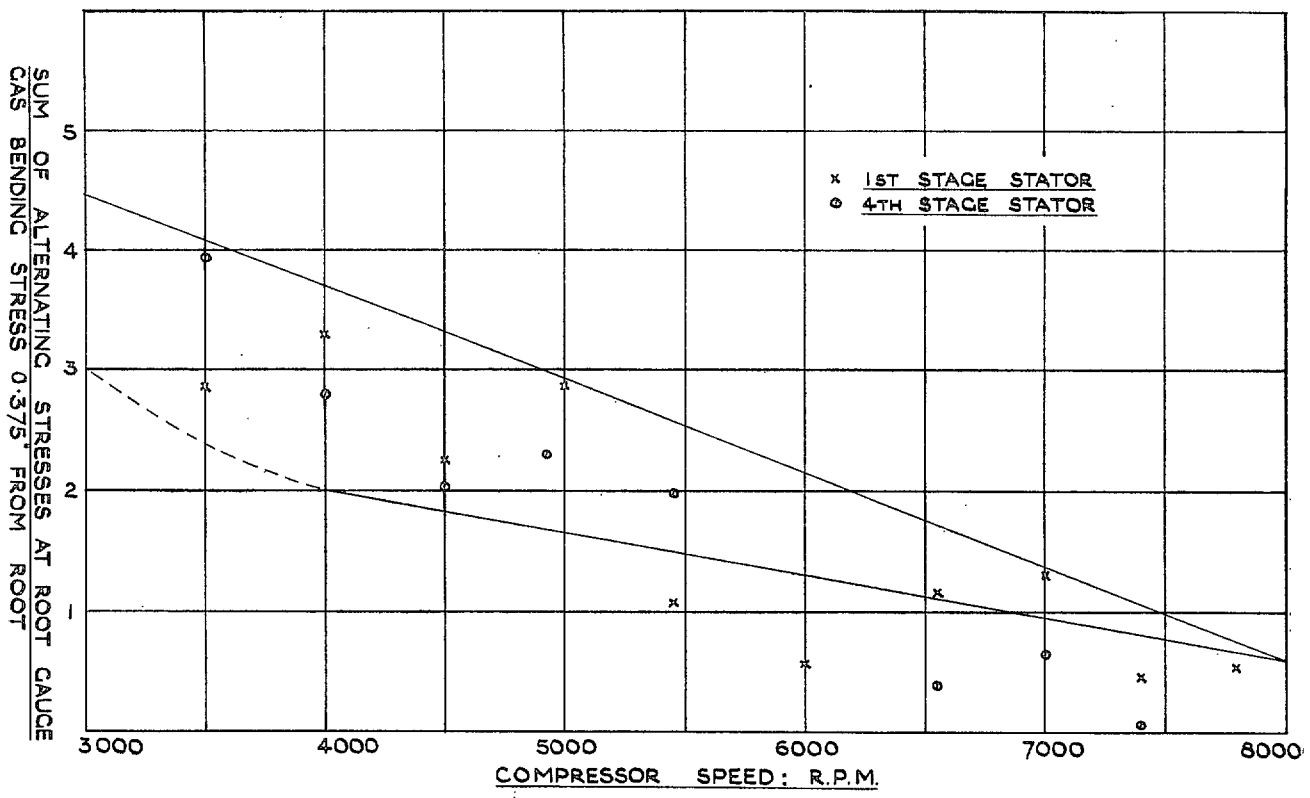

FIG. 20. Ratio of sum of alternating stresses to gas bending-stresses.

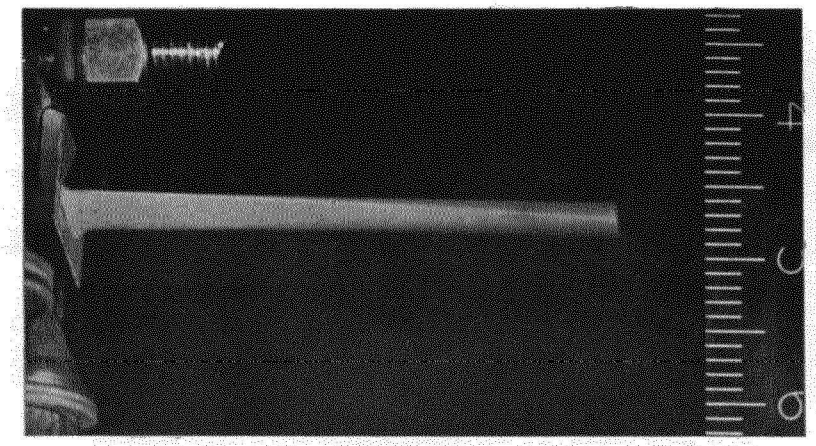

TRAILING EDGE

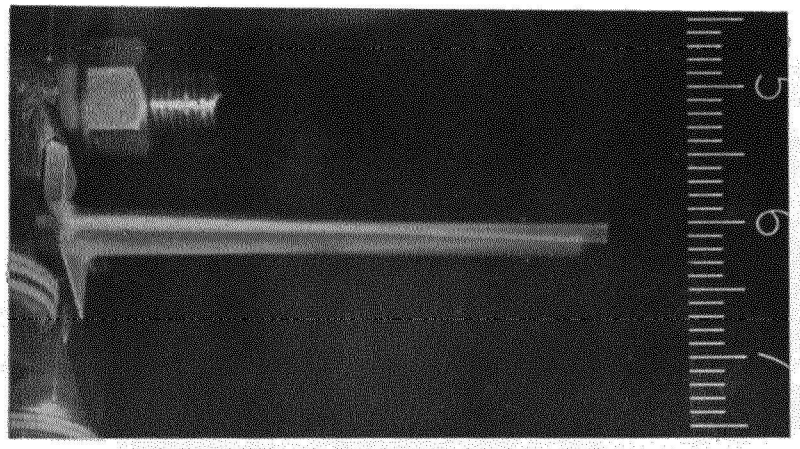

LEADING EDGE

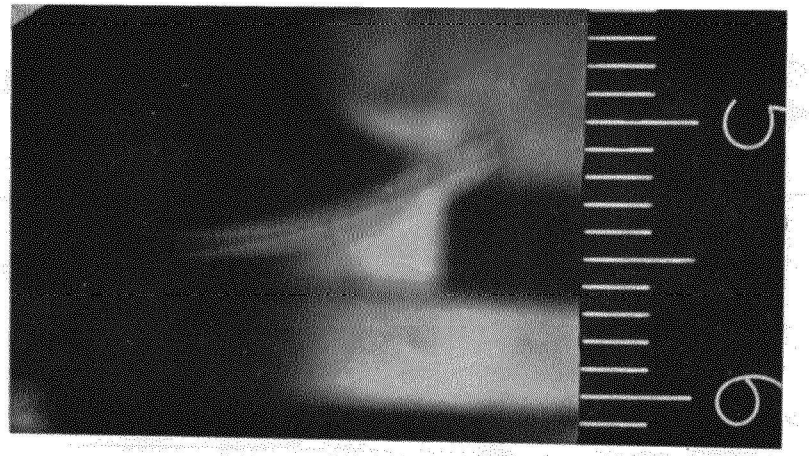

TIP

FIG. 21. Fundamental mode of first-stage stator blade.

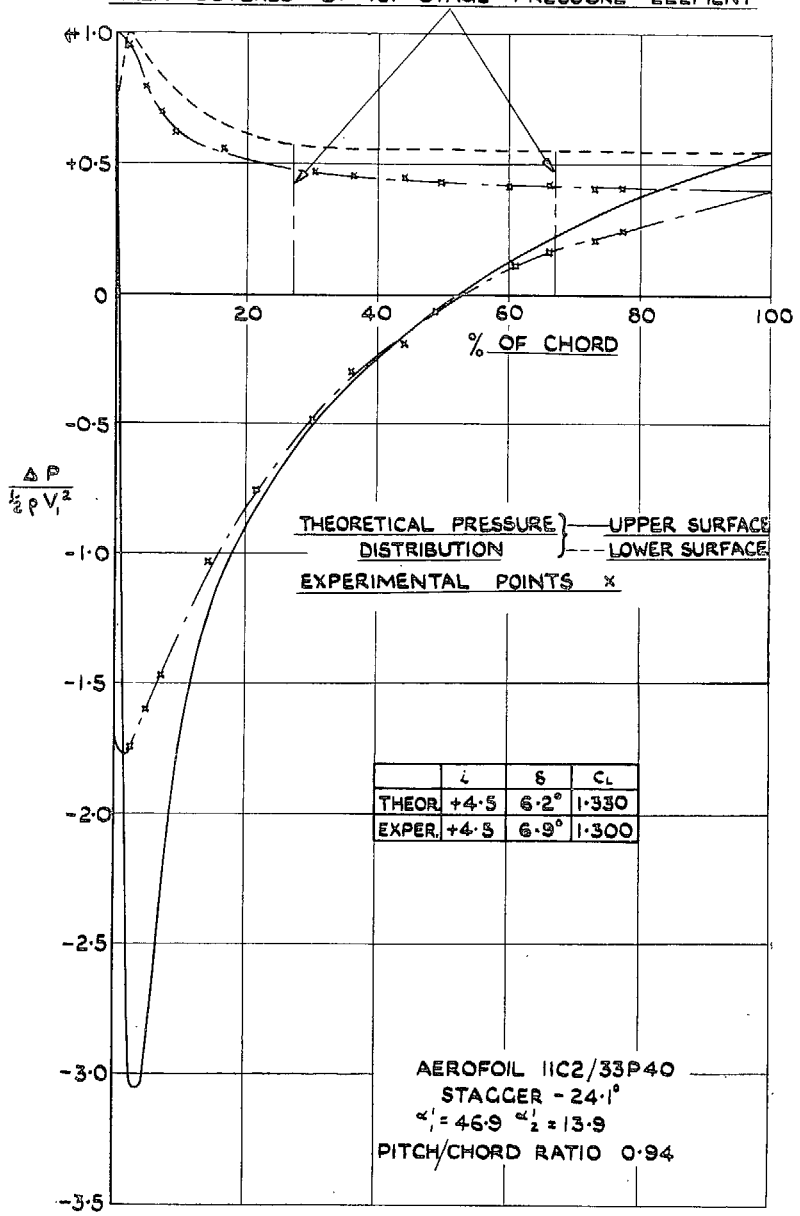

	i	δ	C_L
THEOR.	+4·5	6·2°	1·330
EXPER.	+4·5	6·9°	1·300

FIG. 22. Pressure distribution around aerofoil.

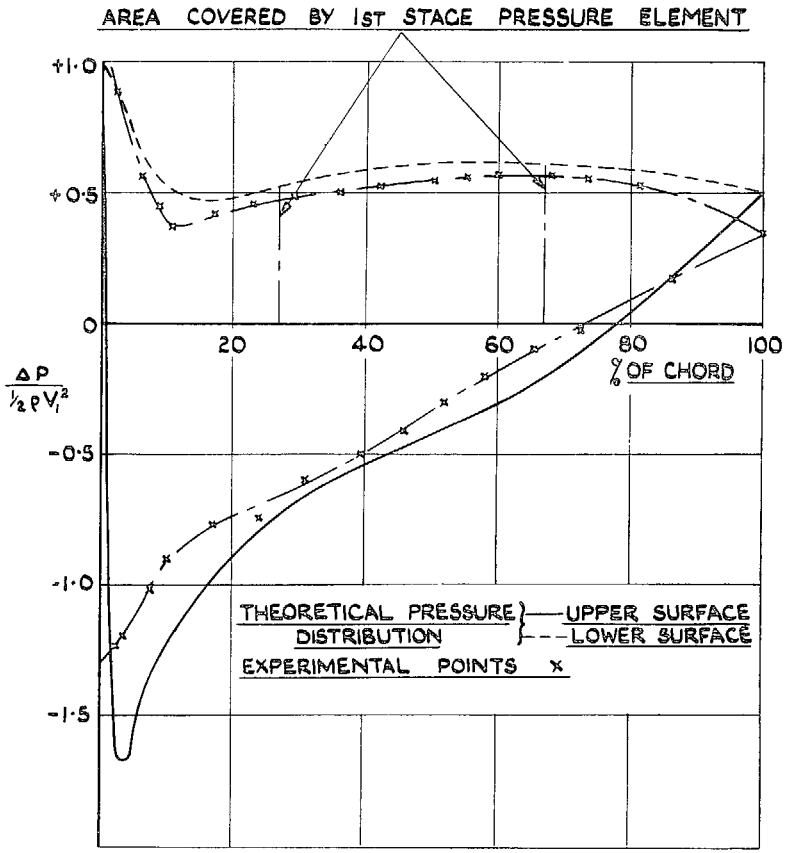

	i	δ	C_L
THEOR.	+1·5	11·7°	1·212
EXPER.	+1·5	12·0°	1·210

AEROFOIL 10C1/40C50
STAGGER - 27·5°
$\alpha'_1 = 47·5°$ $\alpha'_2 = 7·5°$
PITCH/CHORD RATIO 0·94

FIG. 23. Pressure distribution around aerofoil.

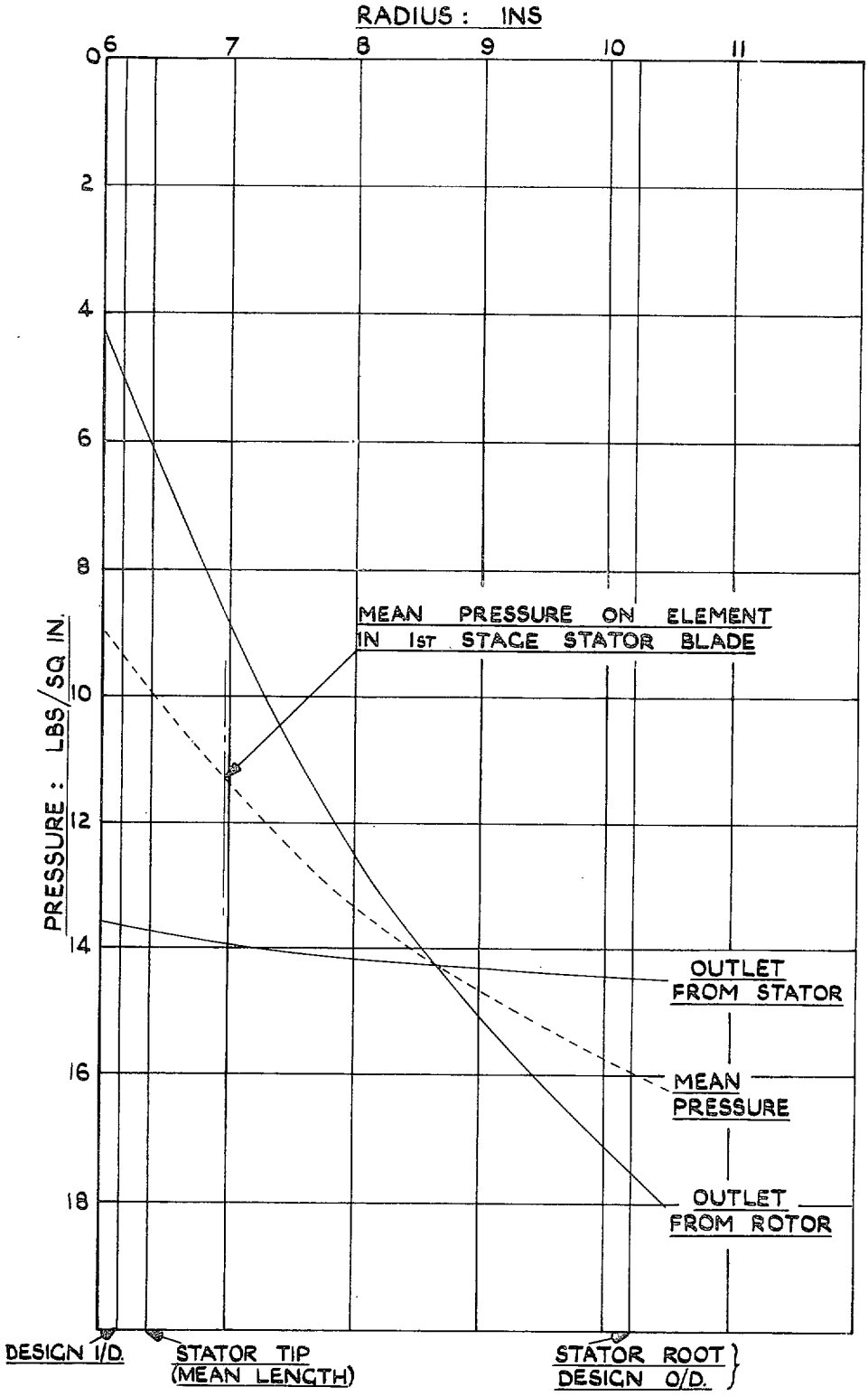

FIG. 24. Estimated mean pressures in first stage.

(6905) Wt. 17/680 K.7 3/56 H.P.Co. 34-261 PRINTED IN GREAT BRITAIN

Publications of the Aeronautical Research Council

ANNUAL TECHNICAL REPORTS OF THE AERONAUTICAL RESEARCH COUNCIL (BOUND VOLUMES)—

1938 Vol. I. Aerodynamics General, Performance, Airscrews. 50*s*. (51*s*. 8*d*.)
Vol. II. Stability and Control, Flutter, Structures, Seaplanes, Wind Tunnels, Materials. 30*s*. (31*s*. 8*d*.)

1939 Vol. I. Aerodynamics General, Performance, Airscrews, Engines. 50*s*. (51*s*. 8*d*.)
Vol. II. Stability and Control, Flutter and Vibration, Instruments, Structures, Seaplanes, etc. 63*s*. (64*s*. 8*d*.)

1940 Aero and Hydrodynamics, Aerofoils, Airscrews, Engines, Flutter, Icing, Stability and Control, Structures, and a miscellaneous section. 50*s*. (51*s*. 8*d*.)

1941 Aero and Hydrodynamics, Aerofoils, Airscrews, Engines, Flutter, Stability and Control, Structures. 63*s*. (64*s*. 8*d*.)

1942 Vol. I. Aero and Hydrodynamics, Aerofoils, Airscrews, Engines. 75*s*. (76*s*. 8*d*.)
Vol. II. Noise, Parachutes, Stability and Control, Structures, Vibration, Wind Tunnels. 47*s*. 6*d*. (49*s*. 2*d*.)

1943 Vol. I. Aerodynamics, Aerofoils, Airscrews. 80*s*. (81*s*. 8*d*.)
Vol. II. Engines, Flutter, Materials, Parachutes, Performance, Stability and Control, Structures. 90*s*. (91*s*. 11*d*.)

1944 Vol. I. Aero and Hydrodynamics, Aerofoils, Aircraft, Airscrews, Controls. 84*s*. (86*s*. 9*d*.)
Vol. II. Flutter and Vibration, Materials, Miscellaneous, Navigation, Parachutes, Performance, Plates and Panels, Stability, Structures, Test Equipment, Wind Tunnels. 84*s*. (86*s*. 9*d*.)

ANNUAL REPORTS OF THE AERONAUTICAL RESEARCH COUNCIL—

1933–34	1*s*. 6*d*. (1*s*. 8½*d*.)	1937	2*s*. (2*s*. 2½*d*.)
1934–35	1*s*. 6*d*. (1*s*. 8½*d*.)	1938	1*s*. 6*d*. (1*s*. 8½*d*.)
April 1, 1935 to Dec. 31, 1936	4*s*. (4*s*. 5½*d*.)	1939–48	3*s*. (3*s*. 3½*d*.)

INDEX TO ALL REPORTS AND MEMORANDA PUBLISHED IN THE ANNUAL TECHNICAL REPORTS, AND SEPARATELY—

April, 1950	R. & M. No. 2600	2*s*. 6*d*. (2*s*. 7½*d*.)

AUTHOR INDEX TO ALL REPORTS AND MEMORANDA OF THE AERONAUTICAL RESEARCH COUNCIL—

1909–January, 1954 . . .	R. & M. No. 2570	15*s*. (15*s*. 5½*d*.)

INDEXES TO THE TECHNICAL REPORTS OF THE AERONAUTICAL RESEARCH COUNCIL—

December 1, 1936 — June 30, 1939	R. & M. No. 1850	1*s*. 3*d*. (1*s*. 4½*d*.)
July 1, 1939 — June 30, 1945	R. & M. No. 1950	1*s*. (1*s*. 1½*d*.)
July 1, 1945 — June 30, 1946	R. & M. No. 2050	1*s*. (1*s*. 1½*d*.)
July 1, 1946 — December 31, 1946	R. & M. No. 2150	1*s*. 3*d*. (1*s*. 4½*d*.)
January 1, 1947 — June 30, 1947	R. & M. No. 2250	1*s*. 3*d*. (1*s*. 4½*d*.)

PUBLISHED REPORTS AND MEMORANDA OF THE AERONAUTICAL RESEARCH COUNCIL—

Between Nos. 2251–2349	R. & M. No. 2350	1*s*. 9*d*. (1*s*. 10½*d*.)
Between Nos. 2351–2449	R. & M. No. 2450	2*s*. (2*s*. 1½*d*.)
Between Nos. 2451–2549	R. & M. No. 2550	2*s*. 6*d*. (2*s*. 7½*d*.)
Between Nos. 2551–2649	R. & M. No. 2650	2*s*. 6*d*. (2*s*. 7½*d*.)

Prices in brackets include postage

HER MAJESTY'S STATIONERY OFFICE

York House, Kingsway, London, W.C.2; 423 Oxford Street, London, W.1 (Post Orders: P.O. Box 569, London, S.E.1); 13a Castle Street, Edinburgh 2; 39 King Street, Manchester 2; 2 Edmund Street, Birmingham 3; 109 St. Mary Street, Cardiff; Tower Lane, Bristol 1; 80 Chichester Street, Belfast *or through any bookseller*

S.O. Code No. 23-2846